Diploma thesis

Characterization of cellulose type I and type II fibers using Atomic-Force Microscopy

performed at the
Institute of Physics
University of Leoben, Austria

by
Franz J. Schmied

under supervision of
Ao. Univ. Prof. Dr. Christian Teichert

refereed by
Ao. Univ. Prof. Dr. Christian Teichert

Leoben, March 2008

To my family

AFFIDAVIT

I declare in lieu of oath, that I wrote this thesis and performed the associated research myself, using only literature cited in this volume.

_____

Franz Schmied

Charakterisierung von Typ I und Typ II Cellulosefasern mit Hilfe der Rasterkraftmikroskopie

Cellulose ist einer der wichtigsten nachwachsenden Rohstoffe unserer Zeit und zugleich die häufigste organische Verbindung der Erde. Dieser Rohstoff kann einerseits für die Papierherstellung als auch zur Textilproduktion verwendet werden. Im ersten Fall handelt es sich dabei um natürliche Cellulose, oder Cellulose Typ I, im zweiten Fall spricht man von so genannter Regeneratfaser oder Cellulose Typ II. Die Rasterkraftmikroskopie (atomic force microscopy – AFM) wurde nun verwendet, um diese beiden Typen von Cellulosefasern näher zu charakterisieren.

Der erste Teil der Diplomarbeit beschäftigt sich mit der Untersuchung natürlicher Cellulosefasern. Hierbei wurden Papierfasern der Firma Mondi Packaging Frantschach GmbH, St. Gertraud, Austria, verwendet, um die Morphologie an der Oberfläche zu charakterisieren. Die Beschaffenheit der Oberfläche ist neben der chemischen Zusammensetzung der Hauptgrund für die Faser – Faser Bindung im Papier. Mit Hilfe von AFM-„Phase imaging“ konnte gezeigt werden, dass sich die Mikrofibrillen, die einen Durchmesser von etwa 40 nm haben, zu Faserbündeln von ca. 300 nm Durchmesser an der Oberfläche anordnen. Weiters konnte der Einfluss der Trocknungsbehandlung sowie der Ozonbehandlung auf die Fibrillenanordnung gezeigt werden.

Der zweite Teil beschäftigt sich mit der inneren Struktur von Textilfasern, die neben der Chemie den größten Einfluss auf die makroskopischen Fasereigenschaften hat. Im Vordergrund stand die Untersuchung der Anordnung der Poren, sowie deren Größe und Form. Hierzu wurden Querschnittsanalysen an Modal-, Viskose- und Tencel®-Fasern der Firma Lenzing AG, Lenzing, Austria, durchgeführt. Um eine dreidimensionale Vorstellung zu erhalten, wurden in weiterer Folge Analysen an Längsschnitten durchgeführt. Mithilfe des AFM-„Phase imaging“ war es möglich, die unterschiedlichen Morphologien der einzelnen Fasern auf der Nanometerskala sichtbar zu machen und die Porengrößen quantitativ zu erfassen.

Characterization of cellulose type I and type II fibers using Atomic Force Microscopy

Cellulose is one of the most important renewable raw materials in recent time and also the most frequently occurring organic compound in the world. This raw material can be used to produce either paper or textiles. In the first case the cellulose is called native cellulose or cellulose type I. In the second case the cellulose is known as regenerated cellulose or cellulose type II. Atomic force microscopy (AFM) was applied to characterize these two types of cellulose fibers.

The first part of the diploma thesis deals with the investigation of paper fibers. Fibers from the Mondi Packaging Frantschach GmbH, St. Gertraud, Austria, were used to analyze the morphological behavior of the surface. The surface arrangement is beside the chemical composition the most important influence on the fiber – fiber bond. With AFM phase imaging it was possible to show the arrangement of microfibrils with diameters of about 40 nm to main bundles with diameters of about 300 nm. It was also possible to reveal the influence of the drying and ozone treatments on the fibril arrangement.

The second part deals with the investigation of the inner structure of textile fibers, which has - beside the chemical composition - the greatest influence on the macroscopic properties. The investigation focused to analyze the distribution of pores, their size and shape. Cross-sectional scans on Modal, Viscose and Tencel® fibers from Lenzing AG, Lenzing, Austria, were done. To achieve a three-dimensional view of the fiber structure, additional measurements on longitudinal cross-sections were performed. By means of AFM phase imaging, it was possible to reveal the different pore structure within the individual fibers on the nanometer scale and to determine quantitatively the pore size.

1. Content

2. Motivation

Cellulose fibers are one of the most used renewable materials utilized in the world. For example, this diploma thesis is written on paper made of bonded cellulose fibers. Other famous products are different kinds of textiles. So everyone uses cellulose fibers and the demand for the corresponding raw material is increasing. In the last decades, the demand for wooden chips and pellets for heating has also increased significantly. This is a big problem for textile and paper industries, because the availability of the raw material will decrease. In particular, paper industry had to reduce the amount of the raw material without losing paper strength. The future aims in packaging industries are to increase the quality and the printability with simultaneous reduction of the production costs [1]. Decades ago, bags for cements needed three layers of paper to secure the cement. Nowadays it is just one layer and it still works (see Figure 1 left). But this is the end of the established design in paper industries. Now, new ideas are needed to increase the paper strength further more with less as possible pulp material. So it is a matter of fact that no one exactly knows how the fibers in paper actually bond. This is the reason why a Christian Doppler Laboratory “For surface chemical and physical fundamentals of paper strength” has been established. The Scanning Probe Microscopy Group at the University of Leoben joined this CD Laboratory to apply Atomic Force Microscopy (AFM) to study paper fibers and fiber-fiber bonds.

Figure 1: Cellulose products:
Left: Cement bag (from [2])
Right: TENCEL® shirt (from [3])

Native cellulose is also known as cellulose type I. “Man-made” fibers are called cellulose type II. That is the reason for the sequencing in this diploma thesis. Actually the history of this diploma thesis started with analyzing cross-sections of textile fibers.

These investigations were based on know-how acquired in a previous diploma thesis [4]. Due to the acquired skills it was possible to expand the work rapidly onto native cellulose.

The starting point for the AFM investigation of native cellulose was to analyze single paper fiber surfaces. To obtain information about the surface chemistry Attenuated Total Reflection Fourier Transformation Infra Red Spectroscopy (ATR-FTIR) was applied by a collaboration partner. By changing between reflective and transmitting mode it is possible to distinguish the chemical properties on the surface and in the bulk material. The AFM data yields information of surface characteristics and allows a deeper insight into the distribution of the cellulose and the lignin. It is also a suited method to study the influence of the different fiber treatments on the fiber morphology. For cross checking the AFM results, Scanning Electron Microscopy (SEM) was used as a cross-linker between the Optical Microscope (OM) and AFM. This morphological information is a prerequisite to study the fiber-fiber bond and gives an appropriate visualization of the bonded areas.

Another important consumer of cellulose fibers is the textile industries because textile industry is not able to supply the world population with textiles if they would only use cotton or wool. Thus man–made fibers have to be used. Figure 2 presents the time line of textile materials used by mankind. A major break-through was the development of the unique nanofibril structure of TENCEL® fiber in the early 1990s [5]. TENCEL®, made from wood pulp cellulose, offers a unique combination of the most desirable properties of man-made and natural fibers: soft as silk, strong as polyester, cool as linen, warm as wool and as absorbent as cotton. Quite simply a “break-through” fiber [6].

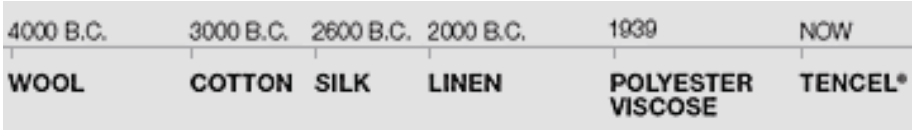

Figure 2: Time scale of textile materials used during history (from [6])

To distinguish the nanostructure of pores, and their shapes it is useful to investigate cross-sectional and longitudinal cross-sectional samples. For achieving this aim, it was helpful to combine AFM and Transmission Electron Microscopy (TEM). On the sub-micrometer scale TEM yields an excellent materials contrast. But to determine pores on the nanometer scale AFM offers a deeper insight and is perhaps able to confess the secrets of the individual textile fibers.

3. Methodological Background

3.1 Composition and hierarchical structure of cellulose fibers

The main components of a cellulose fiber are lignin, hemicellulose and cellulose. Cellulose is an organic compound with the formula $(C_6H_{10}O_5)_n$, a polysaccharide of a linear chain of several thousand linked β-D-glucose units (see Figure 3) [6,7].

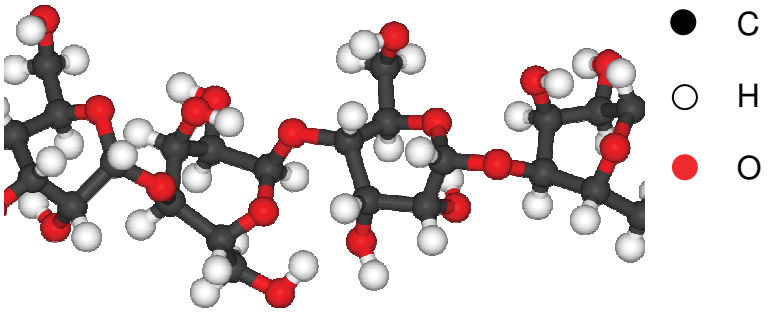

Figure 3: 3D view of a cellulose macromolecule (from [7])

If the macromolecules get close to each other, they build up hydrogen bonds between the hydroxyl group and the hydrogen. These macromolecules bond together to micelles, the basics of the fibrils. The microfibrillar cellulose shows a hydrophilic behavior [8]. Figure 4 presents the schematic assembling of a cellulose fibril.

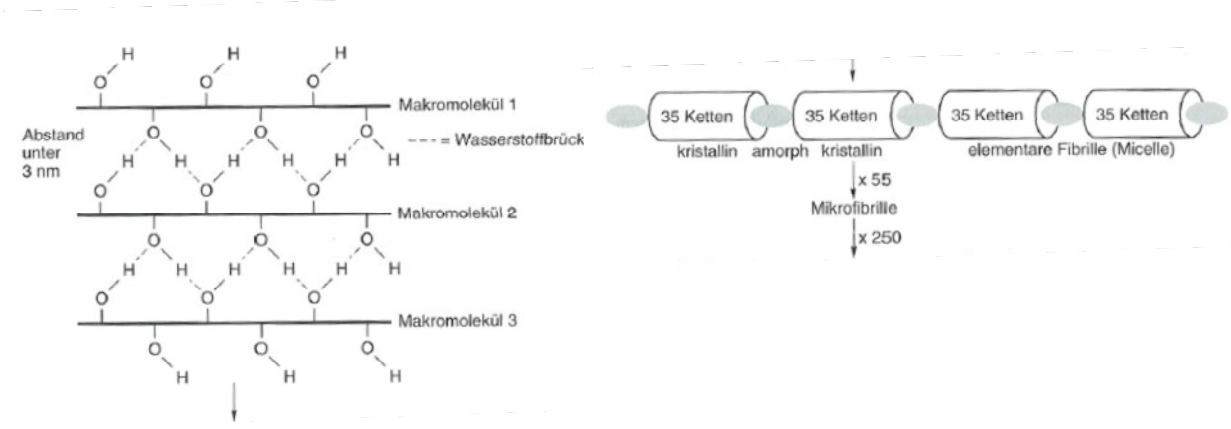

Figure 4: Schematic assembling of a cellulose fibril (from [8])
Left: Macromolecules linked by hydrogen bonds
Right: Micelle, the basic of a fiber

The individual microfibrils are linked by hemicellulose and lignin. Hemicellulose is a slightly branched heteropolysaccharide consisting of different monosaccharide units. Hemicellulose displays a more hydrophilic behavior than cellulose [9].

Lignin is a polymer of phenylpropane units linked to each other in various types of ether and carbon-carbon linkages. Lignin is an amorphous hydrophobic material [9].

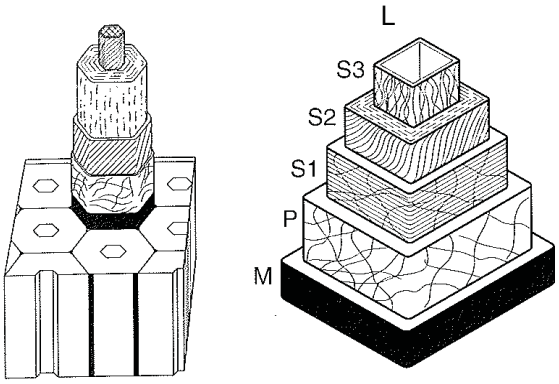

Figure 5: Schematic principle of a fiber cross-section (from [8]) (M: middle lamella, P: primary wall, S1: secondary wall 1, S2: secondary wall 2, S3: secondary wall 3, L: Lumen)

Natural fibers are assembled in different layers. Figure 5 presents the schematic principle of a wood fiber. The first layer is called the primary wall P, and has a thickness of 0.2 µm thin. Here the cellulose chains are disordered. The cellulose chains build some fibrils and are surrounded by lignin.

The next layer is called the secondary wall S1. This layer consists of two cell walls, with a thickness of 0.15 µm. These two walls are assembled by parallel fibrils, which are oriented under certain angles to the fiber axis. The thicker secondary wall S2, which is 5 µm thick, is build up by fibrils, which are oriented in the fiber direction. Lignin and hemicellulose are only found in a low amount. This layer represents 70 % of the whole cell wall seen in Figure 5 [8]. The inner wall, the so called tertiary wall S3 is the finish to the lumen. Concerning the assembling this wall is comparable to the S1 wall.

The hollow space (called lumen L) in the fiber center is necessary for transport of water and nutrients. The lumens of the different cells are connected by a membrane. In living trees the lumen is normally filled up with water [8].

Figure 6a shows an AFM image of a cross-section of a cellulose fiber sample. The left image presents an AFM height measurement. The colors in the image represent the topographical information. Bright features are at a higher position than the dark features as it is presented at the scale bar on the left sight. The height difference

between the brightest and darkest features is 1.5 µm. The right image of Figure 6a presents the corresponding phase image. The colors in the phase image correspond to the phase lag. The dark features display a high phase shift, which means that the tip is strongly interacting with the sample, especially with a water film. The bright features correspond to zero phase lag. The indexed areas in the phase image suggested to be the different layers which are described above. The width of the first layer is about 0.6 µm and belongs to the primary wall and the secondary wall S1. The next layer is the secondary wall S2 with a width of 4–5 µm. The last layer is the secondary wall S3 and is 0.2 µm wide. The lumen is filled with the resin instead of water. The red box in the left image of Figure 6b indicates the comparable size of the AFM image.

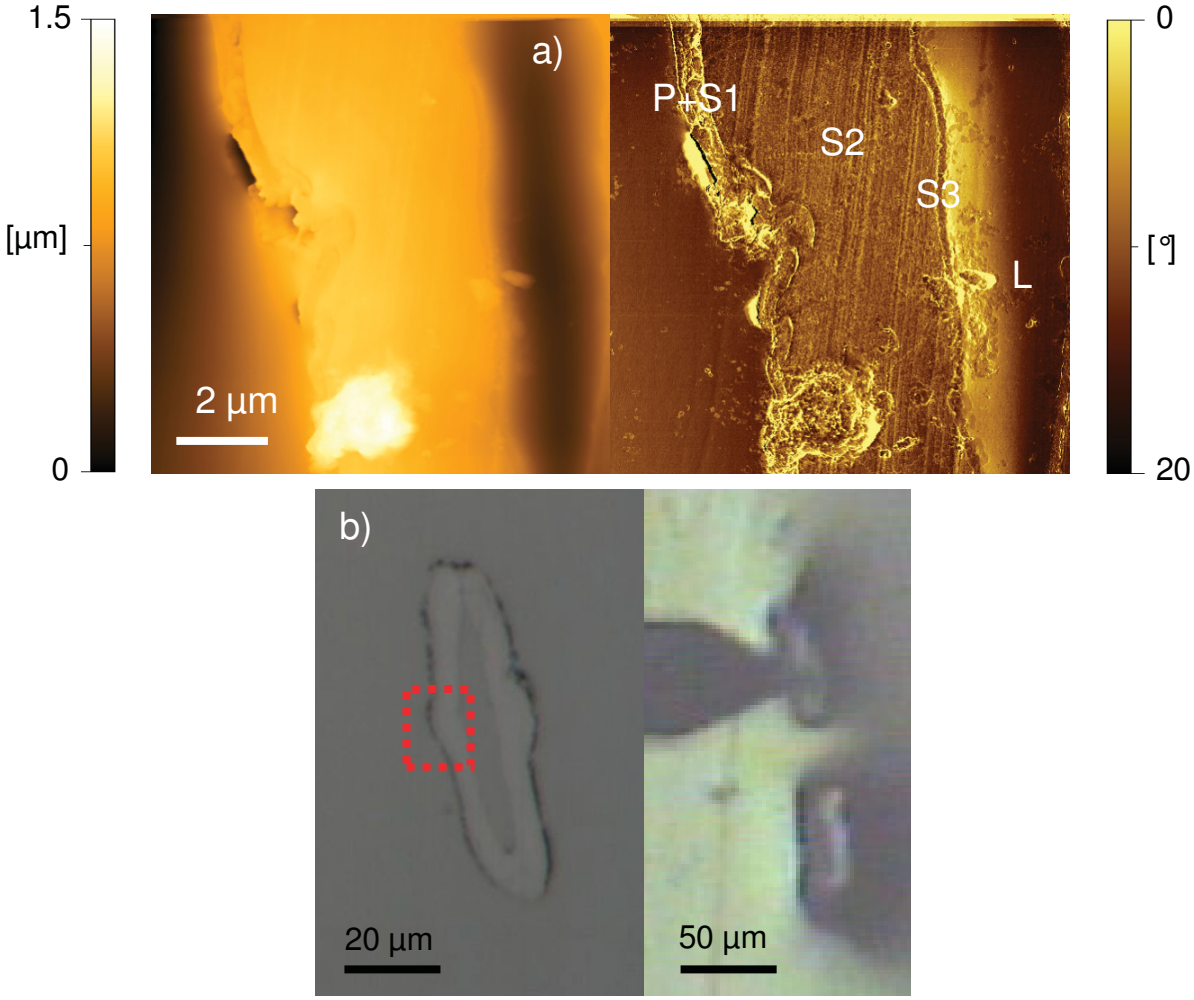

Figure 6: AFM images and OM images of a natural fiber cross-section
a) Height and phase image (z-scale: 1.5 µm, φ-scale = 20 °)
b) Optical image with and without cantilever

3.2 Difference between native and regenerated cellulose

The major difference between these two cellulose types is the orientation of the different layers in the microfibril. If the orientation of the layer is parallel (seen in Figure 7, left), the cellulose is called native cellulose, which is produced in living plants. The thermodynamically more stable version is the antiparallel one, which is found in the regenerated cellulose (Figure 7, right) [11]. To produce regenerated cellulose it is necessary to modify the cellulose fibers chemically [12].

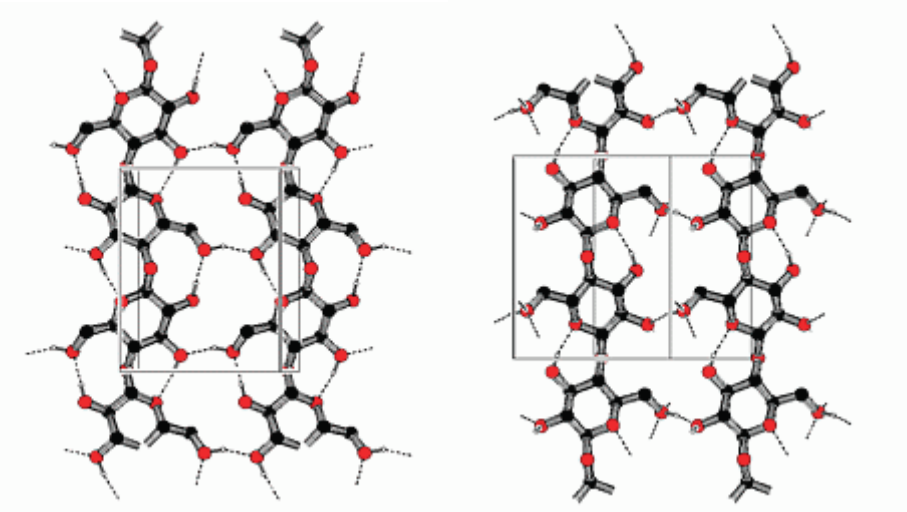

Figure 7: The two major polymorphs of cellulose (from [10])
Left: Native cellulose or cellulose type I
Right: Regenerated cellulose or cellulose type II

There are different fabrication methods for this modification.

- Viscose
- Modal
- Lyocell

The main difference between these three types of regenerated cellulose is the structure of the microfibrils. The chemical composition is the same. The difference in the structure depends on the different production processes. The reactivity of the fibers is mainly determined by two points. One is the fraction of the amorphous and crystalline area, the other is the pore system. The pore system includes pore diameter, shape, and distribution [12].

The Viscose fiber gives the fabric a smooth and pliant handle. The benefits are good wearing, color fastness, and illuminating power. Also brilliance and high flexibility is

given. The Achilles heel is the bad wet strength. The attempt to overcome this disadvantage leads to the developing of the Modal fiber, also known as modified Viscose [13].

The Modal fibers are manufactured in a process which leads to a high strength and a high Young's modulus in the wet state. Also a good absorbance and a high uniformity are given by the Modal fiber. In addition the fiber is skin friendly and has good dyeing properties. Normally the fiber is mixed with cotton or polyester [13].

The TENCEL® fiber is a fiber of the lyocell class. The fiber is breathable and eudermic. TENCEL® in a mixture with other fibers upgrades their properties, gives them a glamorous look and is soft as silk. It is tougher then other cellulose fibers and 100% biodegradable [13]. The mystery behind these wonderful properties should be found in the nanostructure of the fiber. This is the reason why AFM was applied.

3.3 Introduction to Atomic Force Microscopy based techniques

AFM is a scanning probe technique, where a sharp tip (the probe) is scanned across a surface [14]. It is a powerful tool for analyzing solid surfaces on the nanometer scale. The advantage of the AFM is that it is a direct imaging method and it yields true topography information. Figure 8 represents the measuring principle of AFM.

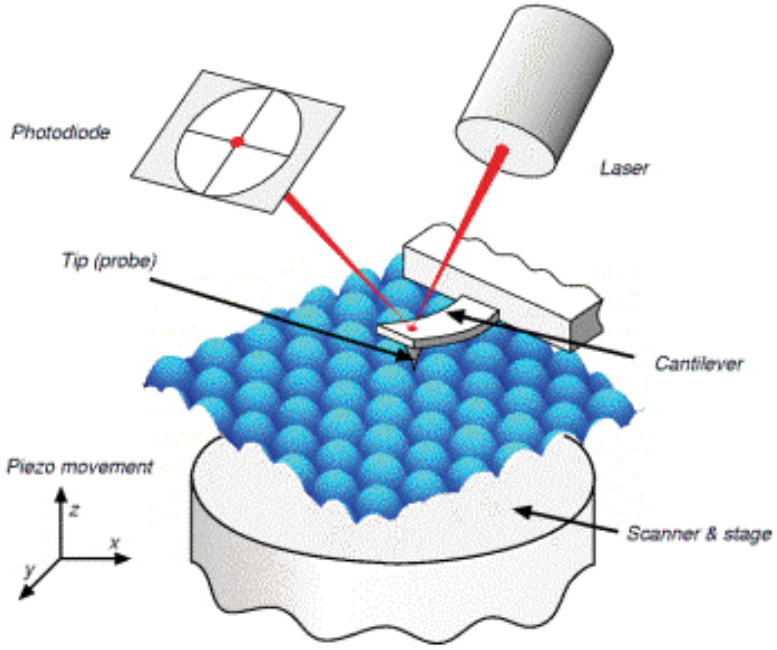

Figure 8: Schematic principle of an AFM (from [15])

The cantilever with an attached tip is laterally moved across the sample driven by a piezoelectric scanner. The deflection of the cantilever, caused by the tip–sample interaction, is detected by a laser beam method (see Figure 8). The z-movement is stored as a function of the lateral position. Actually, this method provides rather a feeling of the surface than a viewing. Therefore, the term “microscopy” is not really correct.

It is now possible to use the probe either in contact mode or in a non-contact mode. A special dynamic mode is the tapping mode, where the probe slightly penetrates the sample.

3.3.1 Tapping Mode

In Tapping Mode (TM), the cantilever is oscillating near its resonance frequency. The cantilevers used for this work were standard silicon cantilevers with a resonance frequency between 200 kHz – 400 kHz. If the tip is interacting with the sample the

cantilever oscillation will change. There will be a damping of the amplitude and a shift of the phase. The controller of the AFM detects the changes in the amplitude and moves the tip vertically in order to keep the amplitude constant. This movement of the cantilever in the z-direction gives the height information as a function of the lateral position. The advantages of AFM-TM compared to the contact mode are the following. There is less damage to the tip and the surface will not be changed during the measurement.

Phase mode measurements monitor the phase lag between oscillation driving the cantilever and the cantilever output signal from the split photodiode. Changes in this phase lag reflect changes in the mechanical properties of the surface. This principle is shown in Figure 9. The image shows two different local regions on the flat substrate (brown). The blue region (B) is made of a different material, and protrudes from the substrate baseline. The yellow region (Y) is flat and shows only changes in materials properties. The blue region will be recognized in the height (*h*) signal (topography), whereas the yellow region will not appear in the height trace. However, both regions will be clearly distinguished from the substrate by recording and plotting the phase signal (Φ) [16]. The blue region shows a stronger phase shift compared to brown matrix whereas the yellow one shows a smaller phase shift. However, during the practical use of this method it can happen that high morphological features with sharp edges can influence the phase measurements. To reveal the difference between a true phase contrast and an imaging artifact it is useful to compare the trace and the retrace signal of the phase image. If both signals are more or less identical, it is a true phase signal.

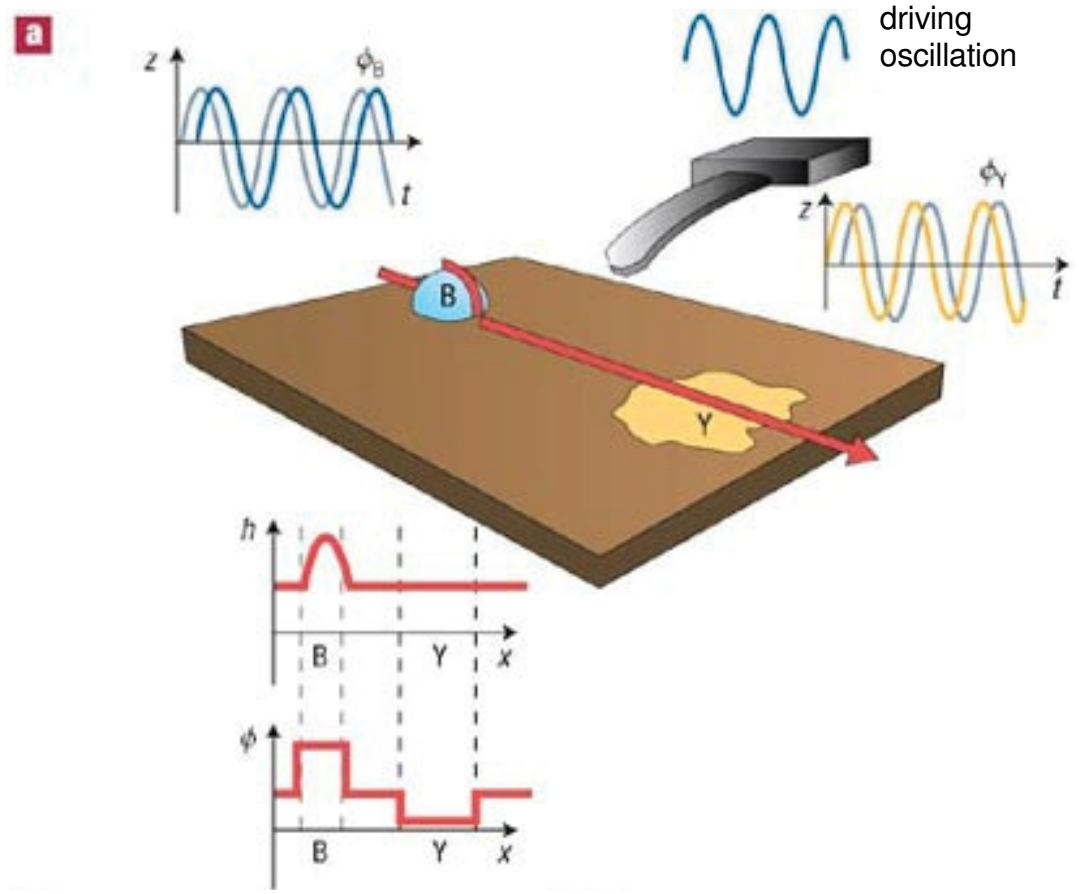

Figure 9: Scheme of the phase-imaging operation (from [16])

This mode was used for all measurements in addition to the height measurements since it allows to detect a difference in the material's hardness. This means that it is possible to detect harder and softer surface areas according to viscoelastic material properties. It is also possible to correlate the phase shift to adhesion forces. A more hydrophil surface results in a greater phase shift. This is used to determine the different building blocks of the fibers, e.g. cellulose, lignin, and hemicellulose. According to Simola et al. [9] lignin is hydrophob. The microfibrillar cellulose shows a hydrophilic behavior and hemicellulose displays a more hydrophilic behavior than cellulose.

3.3.2 AFM image analysis

The software used to analyze AFM data is the Gwyddion software [17]. This free software has the advantage that it is possible to run it on different user systems, e.g. windows, Linux, and it allows to import data files which originate from different AFMs.

Pore Analysis

In the second part of the thesis, pores in textile fiber cross-sections will be analyzed quantitatively. Here, this analyzing procedure is described for pores which are marked with a threshold. It is also possible to do it with a watershed algorithm [18]. However, this does not always work, because of the rough sample surface. Once the pores are marked it is possible to determine the aspect ratio and the angle orientation of the long axis. To determine the aspect ratio we considered the enveloping geometry of the pore cross-section which is also called bounding geometry. This is described in Figure 10.

Maximum bounding size D_{max}: the maximum dimension of the grain in the surface plane. It can be visualized as the maximum width of a gap in the horizontal plane the grain could fill up.

Minimum bounding size D_{min}: the minimum dimension of the grain in the surface plane. It can be visualized as the minimum width of a gap in the horizontal plane the grain could pass through [18].

To improve statistics this analysis procedure is performed for several hundred pores. It is also possible to estimate the average length and width of the pore. The pore aspect ratio is calculated by Equation 3.1 for the individual pores and then averaged.

$$AspectRatio = \frac{D_{\max}}{D_{\min}} \tag{3.1}$$

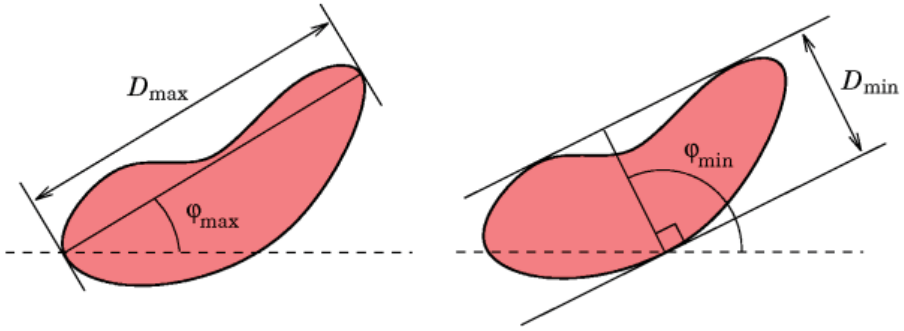

Figure 10: Maximum and minimum bounding dimensions of a grain (from [18])

2D-Fast Fourier Transformation

To analyze a preferred direction and the ordering of the cellulose fibrils, it is useful to calculate the two dimensional Fourier transformation of an AFM image and analyze the brightest spots in the 2D-FFT, which indicates the preferred direction. The width of the structures is the distance between the main spot and the center of the 2D-FFT. Note that the 2D-FFT displays the reciprocal space. Calculation a 2D-FFT is possible with the Gwyddion software. There are different ways to establish a 2D-FFT. For the images in this work the Hann calculation is used.

Note that the Fourier transform treats data as being infinite, thus implying some cyclic boundary conditions. As the real data do not have these properties, it is necessary to use a window function to suppress the data at the edges of the image.

Gwyddion offers several windowing functions. Most of them are formed by some sine and cosine functions that damp data correctly at the edges. For some windowing formulas the independent variable x is from interval [0, 1], which corresponds to the normalized abscissa. For simplicity, variable $\xi = 2\pi x$ is used in the following windowing formula (Equation 3.2). Figure 11 shows various windowing functions.

$$\omega_{Hann}(x) = 0.5 - 0.5\cos\xi \tag{3.2}$$

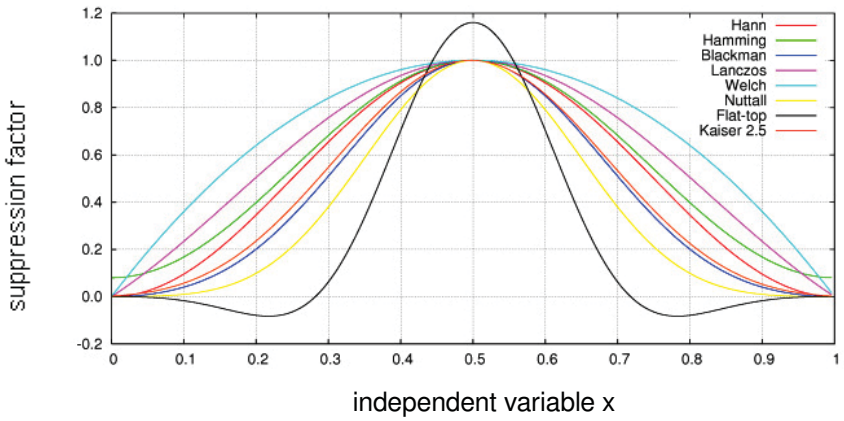

Figure 11: Windowing functions: Hann, Hamming, Blackman, Lanczos, Welch, Nuttall, Flat-top, Kaiser 2.5 (from [18])

Fourier transforms of data with sizes that are not factorable into small prime factors can be very slow – or not implemented at all. Gwyddion can use built-in FFT routines or the famous FFTW library [19] to perform Fourier transforms. In both cases data may need to be resembled to a more FFT-friendly size. This resembling is performed automatically; however, as resembling generally distorts the data, it can result in slightly different outputs of functions that employ FFT, such as PSDF [18].

Determination of the cellulose content

To determine the cellulose content of the paper fibers it is useful to analyze small sections of phase images. This is necessary because the topography influences the phase image. If only the entire image is used for the determination, there are lots of imaging artifacts influencing the value of the cellulose content. To gain more statistics, the bright cellulose is marked with a threshold in several areas. The statistical function from Gwyddion calculates the total (projected) area of marked grains as an absolute value and as a fraction of the total data field area. Then the average of all these areas is calculated.

Figure 12 shows an air dried fiber with a rough surface (see height image in Figure 13). The rms-roughness is 119 nm. The huge roughness of the sample disturbs the determination of the cellulose content. Therefore, only small areas were analyzed. The average value of the analyzed image is 93.2% with a standard deviation of 3.3%. Analyzing the whole image leads to a cellulose value of only 72.1%.

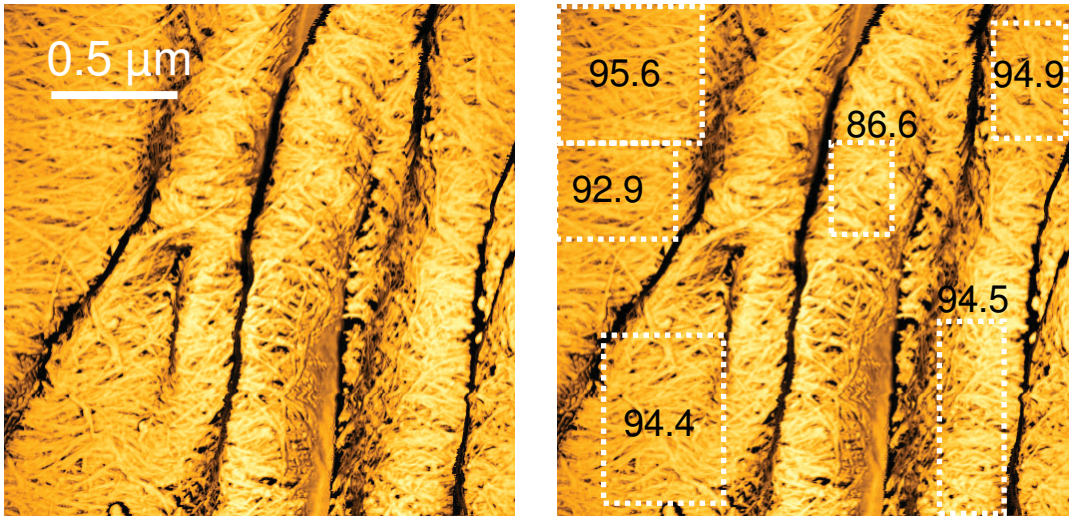

Figure 12: Phase image of an air dried fiber with boxes and the determined cellulose content [%]. (φ-scale: 90 °)

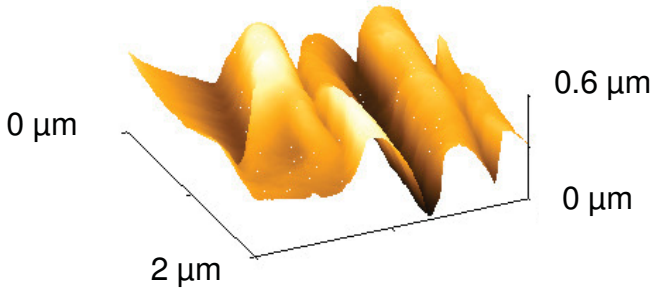

Figure 13: 3D view of the rough height information of Figure 13

3.4 Brief overview on Electron Microscopy Techniques

Scanning Electron Microscopy (SEM) and Transmission Electron Microscopy (TEM) images presented in this work were acquired at the Institute for Electron Microscopy and Fine Structure Research (FELMI) and Graz Centre for Electron Microscopy (ZFE Graz). TEM was applied on ultra-thin cross-sections of fibers to visualize the main characteristics of the internal morphology of man-made cellulose fibers. The images are presented here to give an impression and should confirm the AFM data. To reveal a clear contrast between the cellulose assembly and the pores, the pores are filled with a polymer called isoprene. To have a better contrast in the TEM, the samples were stained with OsO_4 [20]. This osmium treatment leads to a hardening of the surface and may disturb the AFM phase imaging. Therefore, usually samples without OsO_4 treatment were analyzed in AFM.

SEM is a tool for analysis on the micrometer scale. The assembly of an SEM (see Figure 14) is similar to an ordinary optical microscope (OM). Instead of visible light with wavelengths longer than 300 nm, electron beams are used that have - according to the wave-particle Dualism - much smaller wavelengths allowing resolution on the nanometer scale. To achieve the magnification, magnetic lenses are used instead of the glass lenses.

In SEM an electron beam is scanned across the sample. There are two different ways for the electrons to interact with the sample.

- Back scattered electrons
- Secondary electrons

The back scattered electrons give a material's contrast. The back scattering coefficient depends on the ordinal number and the incidence angle. The higher the ordinal number, the more intensity is visible and the brighter is the point on the screen.

The secondary electron emission gives an idea of a topographic contrast. However, the contrast depends also on the angle of the areas and the higher emission at the edges [21]. Thus, SEM yields easy material's contrast but no reliable topography information on the nanometer scale. The lateral resolution from SEM is 50 – 200 Å.

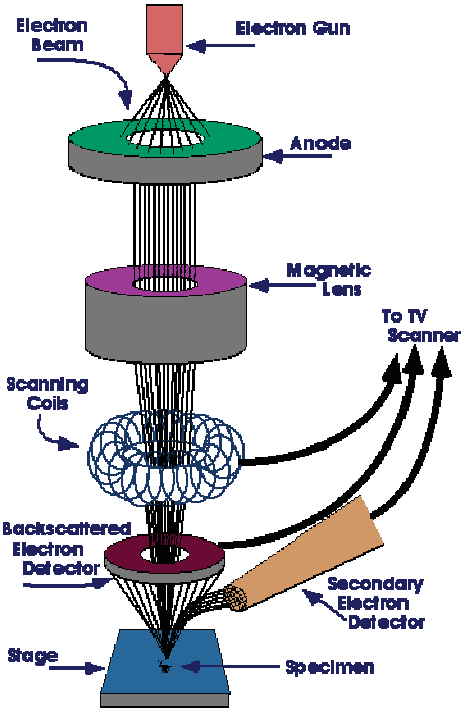

Figure 14: Schematic principle of an SEM (from [22])

TEM is an imaging technique which requires very thin samples. The assembling is similar to an SEM (see Figure 15). The thickness depends mainly on the ordinal number, acceleration voltage and the required resolution. The electrons are scattered in the sample. The higher the ordinal number or the sample thickness the more scattering appears [23]. For TEM images the lateral resolution is about 5 – 20 Å [21].

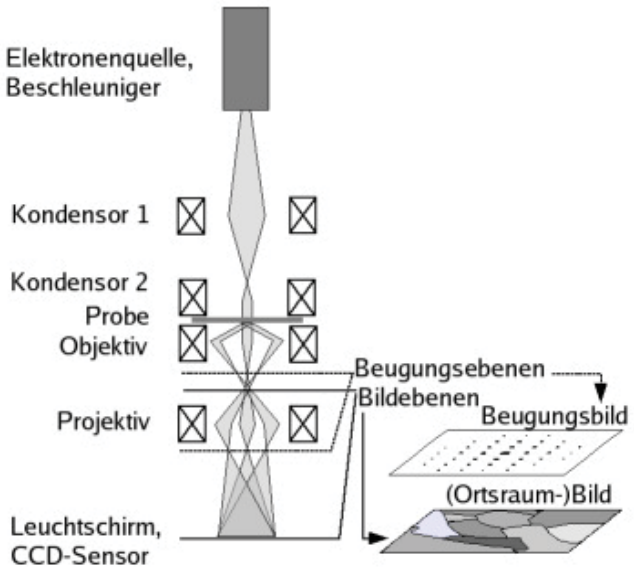

Figure 15: Schematic diagram of a TEM (from [23])

4. Experimental

4.1 Sample preparation

The investigated paper samples were standard kraft pulps from Mondi Packaging Frantschach Gmbh, St. Gertraud, Austria. Monopol is the brand name of high-grade fibers. The raw material is completely made from European conifers, such as spruce and pine. The pulp has a high strength and excellent mechanical and chemical purity. The measurements involved analyzing the surface of differently dried fibers and an ozone treated fiber. A preliminary inspection on cross-sectional samples was also done.

The investigation of the textile fibers involved analyzing cross- and longitudinal sections of Viscose, Modal and TENCEL® fibers provided by the Lenzing AG, Lenzing Austria.

The samples for characterizing the fiber surface are prepared in the laboratory at the Institute of Physics. The single fibers were put on a piece of silicon wafer (5x5 mm²) and fixed with an adhesive tape (see Figure 16).

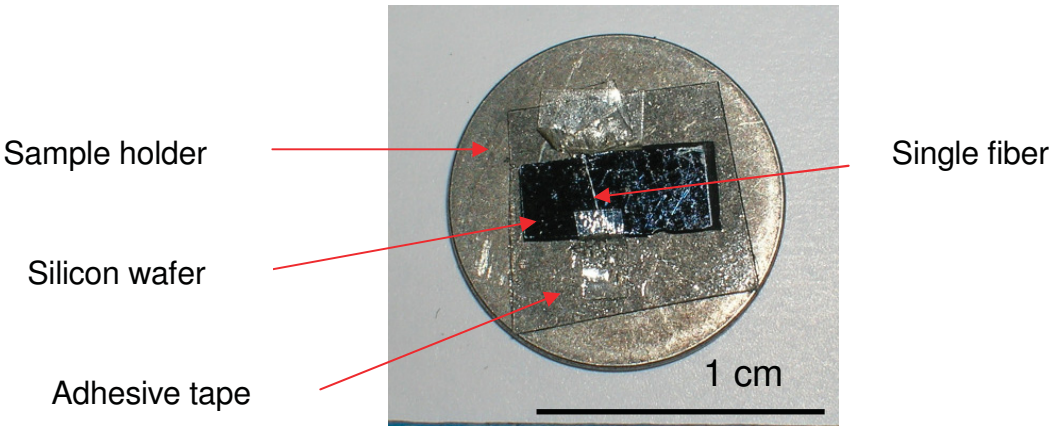

Figure 16: Single fiber sample on a silicon wafer

All the measurements were done under ambient conditions. The temperature was about 21 °C and the humidity ranged from 20 to 50%. One of the major problems with respect to measuring the fiber surfaces was that it is not possible to place the single fiber absolutely flat on the silicon wafer. Figure 17 shows the fiber lying on a silicon wafer. The lower fiber is the mirror image of the fiber. The mirror plane indicates the beginning of the silicon wafer. It is clearly visible that the fiber is only at a few points in contact with the silicon surface.

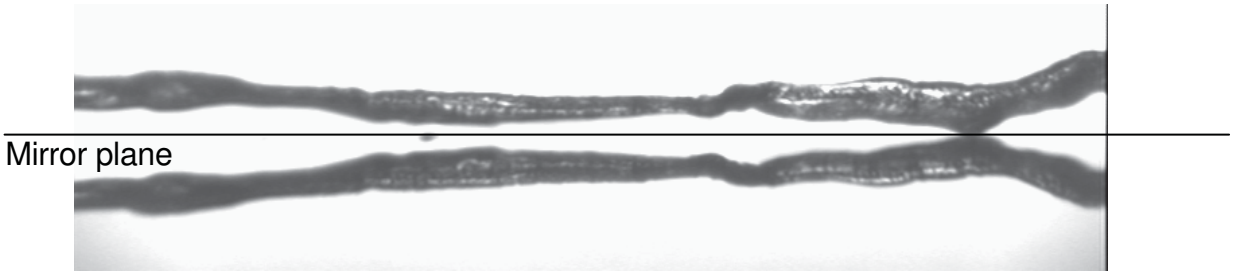

Figure 17: Optical vertical section of a fiber

The cross- and longitudinal sections were prepared at the FELMI in Graz. There, the single fibers were embedded into a resin and then cut under a microtome (see Figure 18 and Figure 19). For using the samples in the Digital Instruments Nanoscope IIIa, it was necessary to make them thinner. This was done with a scalpel by cutting the upper 3 to 5 mm from the embedded sample as it is mentioned in Figure 19. The sample pieces were stuck on a sample holder.

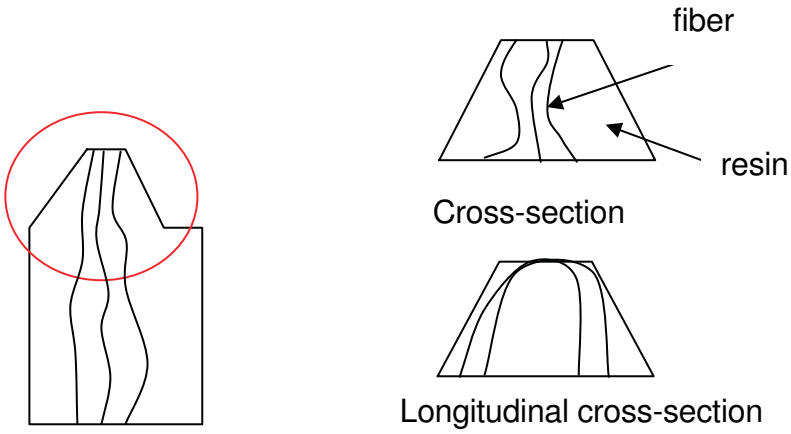

Figure 18: Schematic principle of an embedded fiber for a cross-section and a longitudinal cross-section

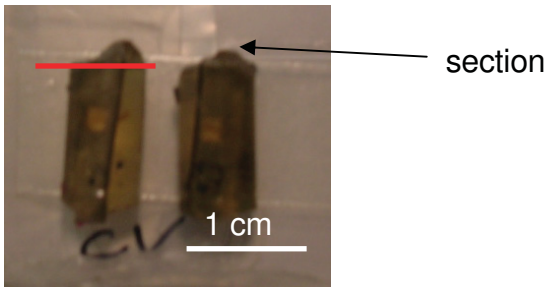

Figure 19: Embedded fiber samples in a resin

To use the samples in the Asylum Research 3D MFP, a special sample holder was designed. This design avoided additional sample preparation damage because the sample is just put in the sample holder. To fix the sample in the holder, plasticine is used.

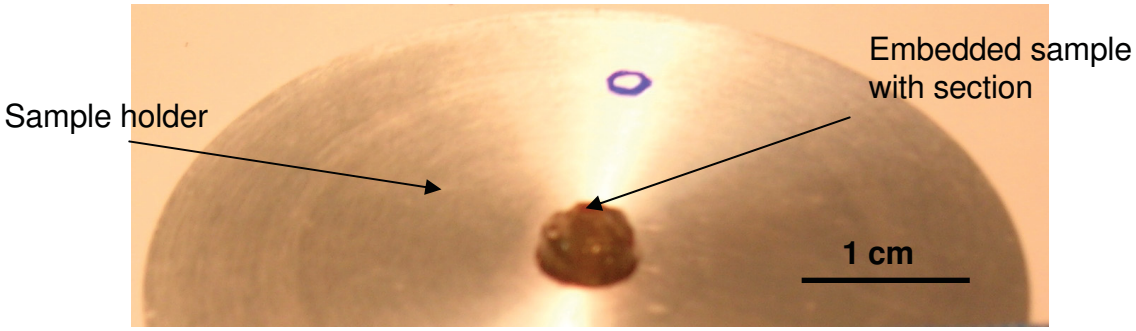

Figure 20: Embedded fiber sample inside the sample holder for the Asylum Research 3D MFP investigation

4.2 AFM measurements

The AFMs used for this work are a Digital Instruments Nanoscope IIIa Multimode AFM (see Figure 21 left) equipped with an AS-130 (J) Piezo Scanner and an Asylum Research MFP 3D (see Figure 21 right). The advantages of the MFP 3D over the DI Nanoscope IIIa is that it has a closed loop scanner and a higher z-limit. This means that it is easier to retrieve an exact position on the sample and allows measuring rougher samples.

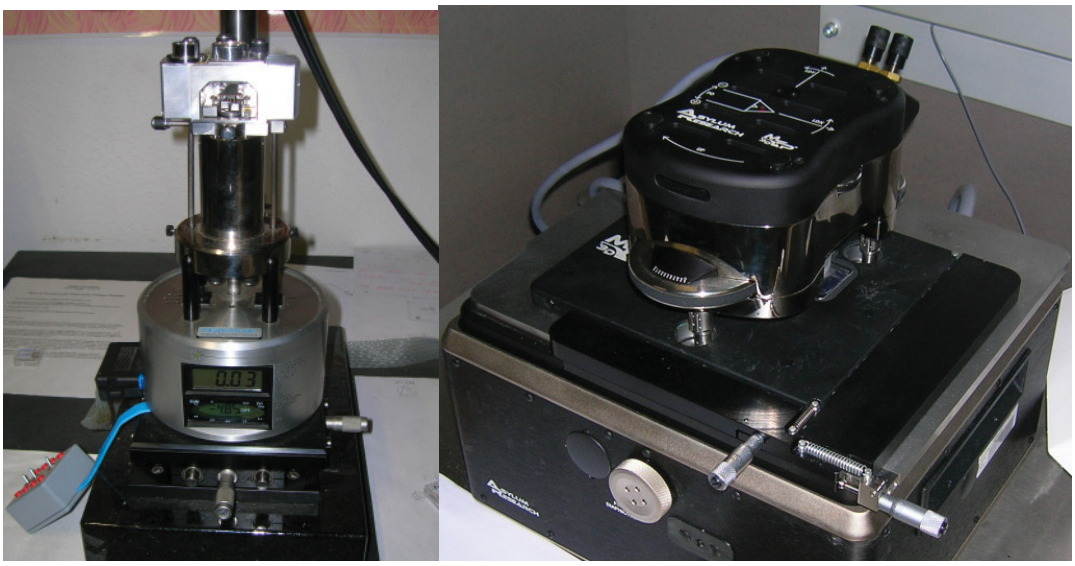

Figure 21: AFMs used in this work:
Left: Digital Instruments Nanoscope IIIa
Right: Asylum Research MFP 3D

All the AFM measurements were performed in Tapping Mode (TM). Measurements showed that there is a difference between “light tapping” and “moderate tapping” according to Simola et al. [9]. Normally, the presented images were recorded in light tapping mode. The moderate tapping sets in very abrupt. Figure 22a shows a height image with visible indents from the tip. These indents are also seen in the phase image as dark spots (Figure 22b). To get a better overview, masking of the dark spots in the phase image was done and put over the height image data (Figure 22c). It shows the perfect fit of the indents in the height image with the dark spots in the corresponding phase image.

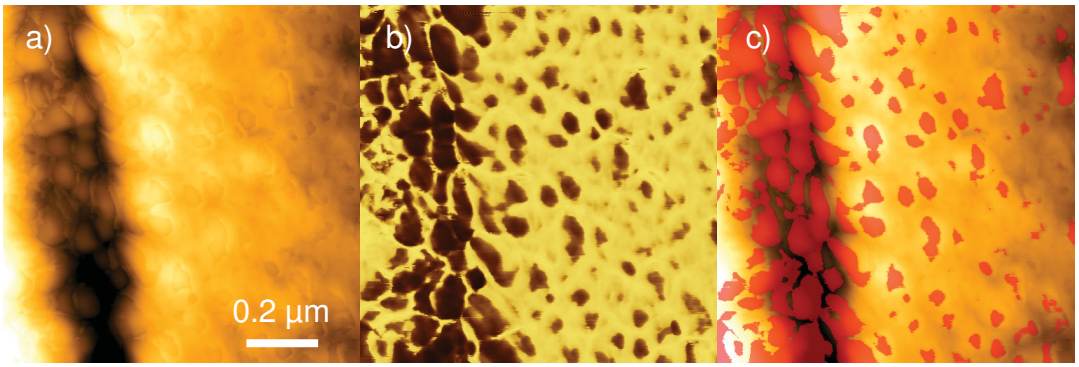

Figure 22: Moderate tapping on a TENCEL® fiber
a) Height image with indents (z-scale: 25 nm)
b) Corresponding phase image (φ-scale: 60 °)
c) Height image with mask from the phase image

4.3 AFM probes

The probes used for this work are standard silicon tips. For measurements using the DI Nanoscope IIIa, Nanosensors PPP-NCHR-50 probes were used. The typical dimensions of the silicon cantilever are 145 µm by 40 µm by 4 µm. The resulting resonance frequency of the cantilevers is between 204 and 497 kHz. The half cone angle of the tip apex is 10°and the typical tip radius is less than 7 nm. On the backside, these cantilevers are aluminum coated for a better reflectivity. These probes have been found to allow stable measurement conditions.

In the Asylum Research MFP 3D, Olympus AC 160 TS probes were used. These silicon cantilevers have a resonance frequency between 284 and 392 kHz. The dimensions of the cantilever are 160 µm by 50 µm by 5 µm. The half cone angle is 6° along the cantilever axis. The radius of the curvature is less than 15 nm. These probes are also coated with an aluminum film for a better reflectivity on the detector side.

In addition, attempts with Nanosensors ATEC tips [24] were undertaken. Figure 23 shows such a cantilever. The advantage is that the exact position of the tip on the sample surface can be observed with the optical microscope attached to the AFM. The resonance frequency for these cantilevers is between 210 and 490 kHz. The dimensions of the cantilever are 160 µm by 45 µm by 5 µm. The half cone angle is less than 12° along the cantilever axis and less than 8° from the side view. The typical tip radius of curvature is less than 10 nm. These ATEC tips don't have a reflective coating on the detector side. The tips show a good measurement behavior in the DI Nanoscope IIIa. For the Asylum Research MFP 3D, there was too much signal loss because of the missing reflective coating.

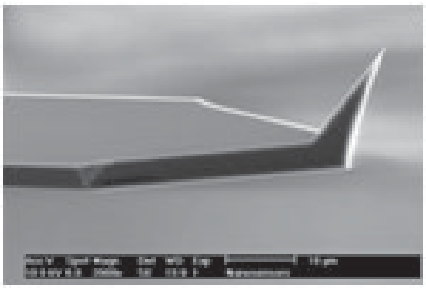

Figure 23: SEM image of an ATEC tip which is located at the very end of the cantilever (from [24])

4.4 Positioning of the cantilever on the fiber

To locate the fibers positioned in the AFM, an Optical Microscope (OM) was used (see Figure 24). For working on the Digital Instruments IIIa an OM from Nikon with an amplification of 10 was used. To store the optical information, the OM was equipped with a CCD camera. A similar system was used at the Asylum Research MFP 3D. This system is necessary for positioning the tip exactly on top of the fiber under investigation with the micrometer screws. Then, the automatic tip approach is used. Nevertheless, several adjustments have to be undertaken to meet the desired sample position.

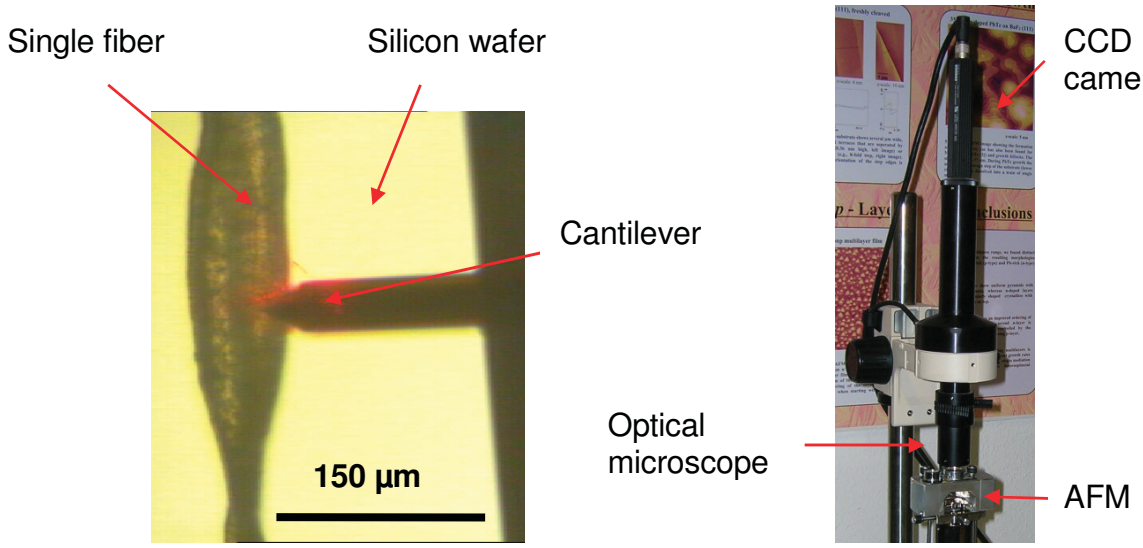

Figure 24: Left: AFM probe positioned over a textile fiber in the DI Nanoscope IIIa
Right: Used optical microscope with CCD camera

5. Results and discussion

5.1 Surface morphology of paper fibers

First, measurements were done on an air dried Monopol E fiber. The analysis was focused on the surface of the fiber. Due to the drying conditions, the surface shrinks and in this case the surface is really rough with wrinkles. It looks like an apple, which lied too long in the sun.

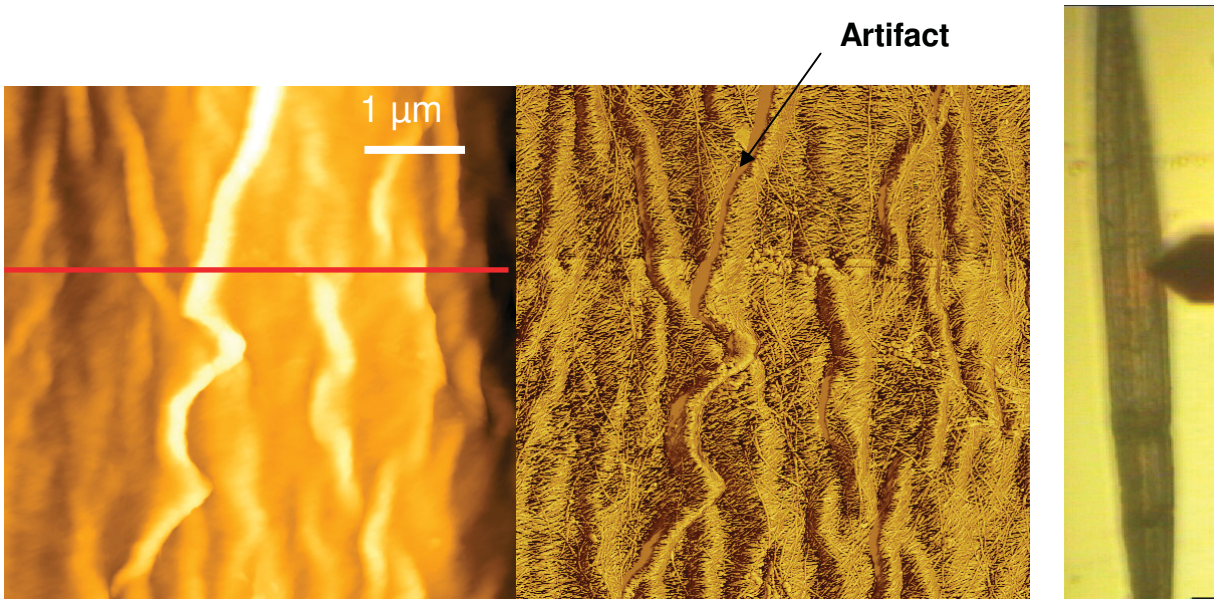

Figure 25: Images of an air dried Monopol E fiber
Left: Height image (z-scale: 500nm)
Middle: Corresponding phase image (φ-scale: 90 °)
Right: Corresponding optical image

The height image in Figure 25 shows a Monopol E fiber. The width of the main bundles of microfibrils is about 300 nm. Similar results have been found for pine and birch pulps [9]. The topographic image also gives a quick hint that there are some features that are a magnitude lower in height, but which are not clearly visible in the topography. Figure 26 presents the line section from the height image of Figure 25, showing the huge roughness of the sample and cross-sections of the individual main bundles of microfibrils.

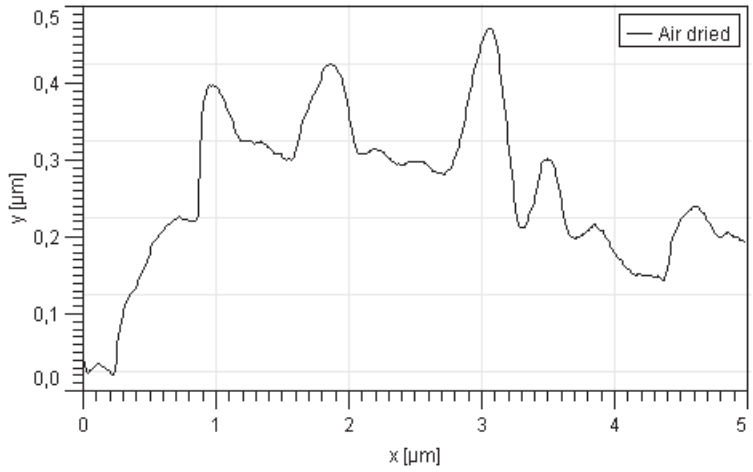

Figure 26: Line section from the red line in the height image of Figure 26

The phase image of Figure 25 shows some bright fibrils and a dark amorphous matrix. The bright features have a smaller phase shift. That means that these fibrils are more hydrophobic than the dark matrix. According to Simola et al. [9] and Gustaffson et al. [25], the bright features are considered to be cellulose. The surrounding linkage is either lignin or hemicellulose. According to [9] it is assumed to be hemicellulose, which is more hydrophilic than cellulose. The width of the fibrils is about 40 nm (see Figure 29). This is in good agreement with the value found in the literature [9,25]. The orientation of the microfibrils is mainly perpendicular to the main bundles of microfibrils.

The large bright stripes seen in the phase image are imaging artifacts due to the abrupt height differences. Due to the lateral scanning, the tip can't follow those steep downward slopes and loses the contact to the sample. Another problem to consider is that the fiber surface is not plane parallel and that the fiber does not lie flat on the surface (demonstrated in Figure 17).

As can be seen in Figure 27, SEM images reveal the same two features but not with such a clear contrast. Nevertheless, SEM is a good method to check the AFM data. The main bundles of microfibrils and the microfibrils itself seen in the AFM are also visible in the SEM images and their determined size is in the same order of magnitude. In the SEM images, the features are a little bit smaller than in the AFM image. This is due to the imaging technique. An AFM tip is not infinitely sharp; the tip has a certain opening angle and tip radius. This leads to a tip-sample convolution [26]. That means that the features seen in the AFM are a little bit overestimated in terms of size.

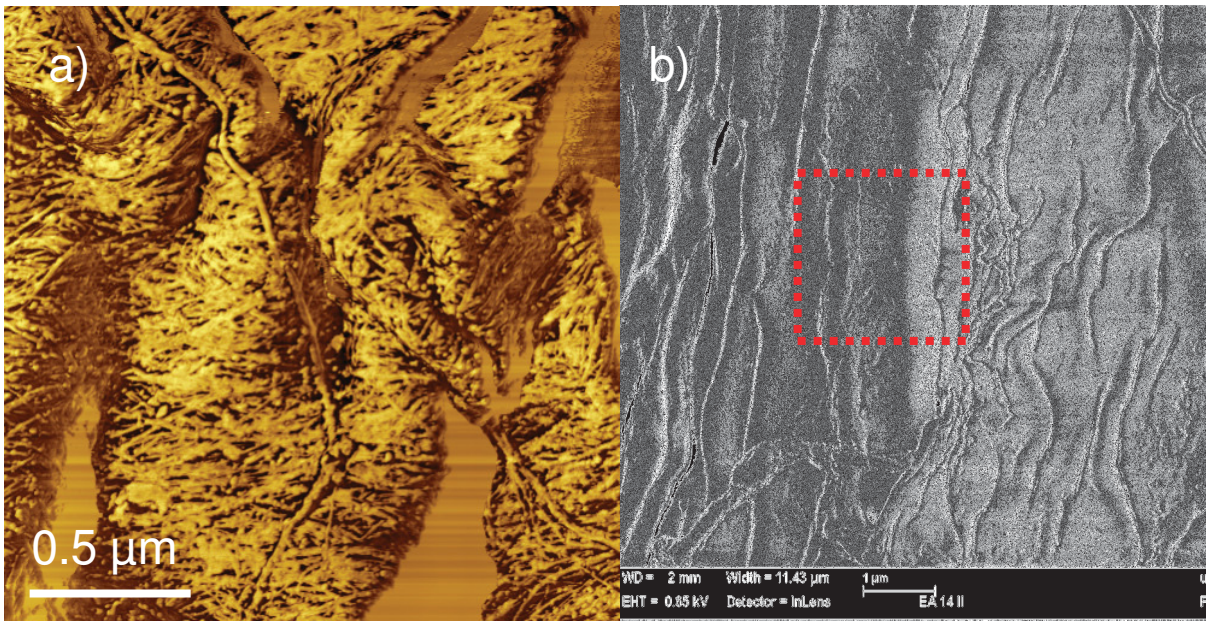

Figure 27: Comparison of an a) AFM phase image and b) SEM image of a Monopol E paper fiber

The 2µm x 2µm box marked in red in Figure 27 b) indicates the comparable size of the AFM image. It is clearly visible that the AFM image reveals a better contrast. The cellulose fibrils seen in the SEM have a diameter of about 30 nm. In the AFM image the diameter is about 40 nm, due to the finite tip.

The SEM scans are done at the FELMI, Graz, without coating of the fiber. The images show a good quality and predict the AFM data. SEM is a well-suited method to analyze the fibers on the micrometer scale, but to investigate on the nanometer scale AFM yields more details, because AFM yields true topography information instead of SEM and reveals a material's contrast during phase mode measurements. SEM is an appropriate tool to have a quick overview on the fiber surface.

5.1.1 Different drying methods

In the following, the influence of the different drying methods is investigated. There are several different drying methods. The easiest method is to dry fiber samples in air. Others are flash drying or freeze drying methods. Figure 28 shows a comparison between the AFM results of air dried and flash dried Monopol E fibers.

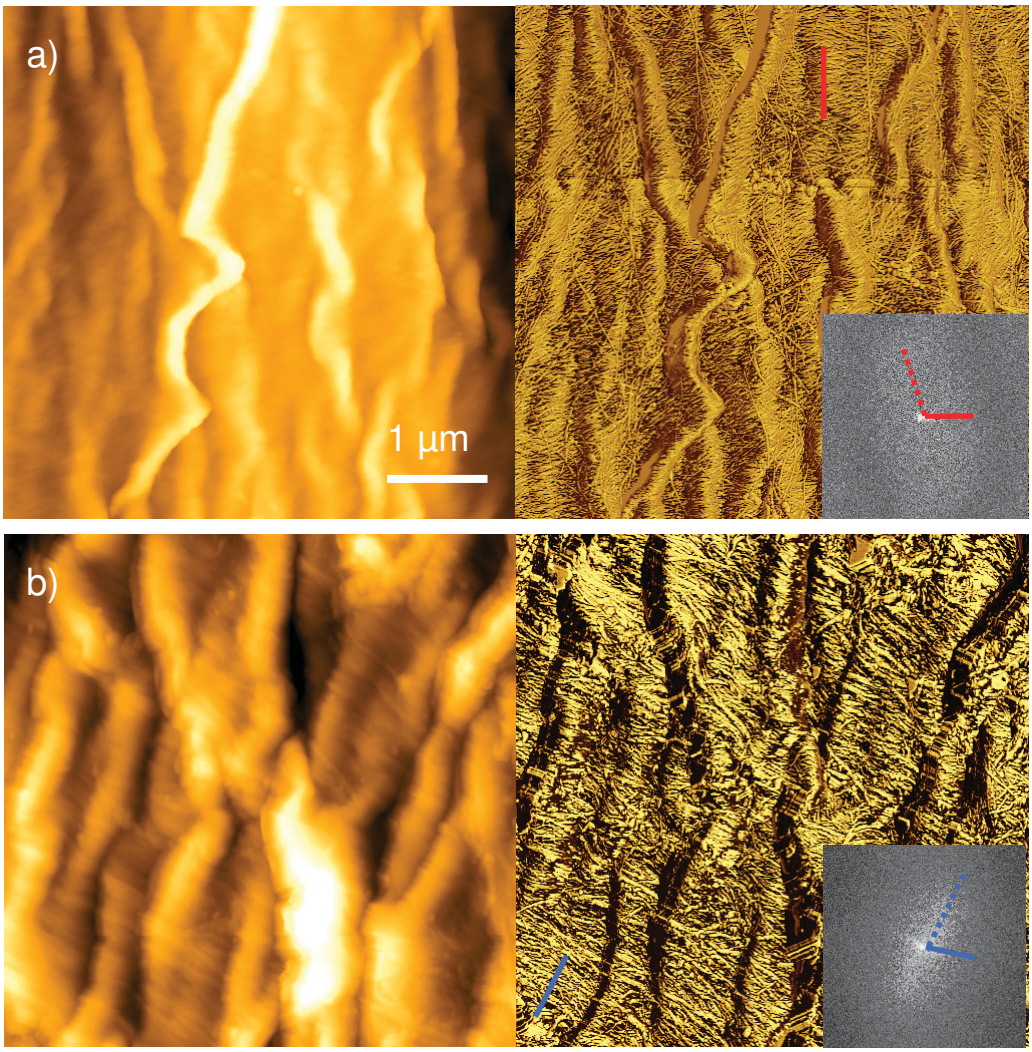

Figure 28: AFM images of a) an air dried and b) a flash dried Monopol E fiber
Left: Height image (z-scale: 500 nm)
Right: Corresponding phase image (φ-scale: 90 °)
Insets: Corresponding 2D-FFT from the phase images

The surface roughness of the two different drying processes appears to be the same. The air dried fiber has an rms-roughness of 88 nm. For the flash dried fiber it is 94 nm. Since the roughness is in the same range, it is possible to compare the two phase images quantitatively.

Analysis of the phase images of air dried fibers according to the procedure presented in Figure 12 reveals a higher average cellulose value of about 74 ± 5%. For the flash dried fiber the content is about 59 ± 4%. The difference between the average cellulose content is may be due to the fluctuation in the individual fibers. The inserted 2D-FFTs give an idea of the preferred fiber direction. The cellulose fibrils are running more or less perpendicular to the main axis of the microfibril bundles. The typical width of these fibrils is 27 ± 7 nm for the air dried fiber and 44 ± 9 nm for the flash dried one (see Figure 29). The measurements show that there is no such big difference between these drying methods, concerning the surface structure. The air dried and the flash dried fibers show a similar arrangement of the individual fibrils on the fiber surface.

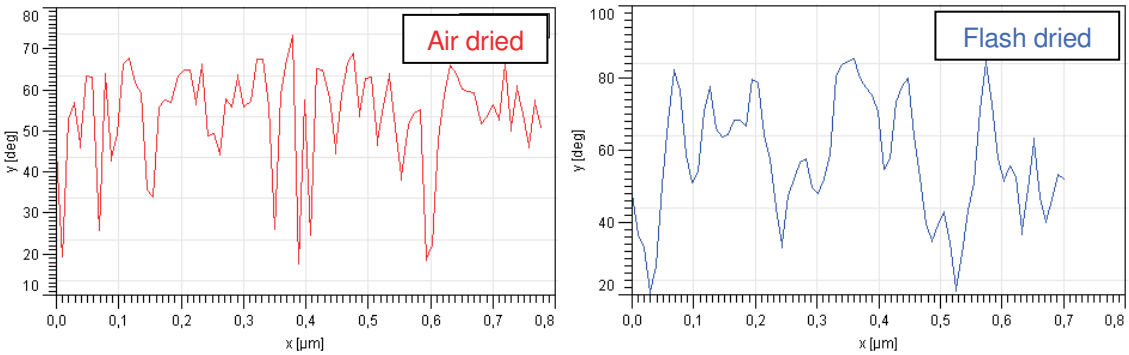

Figure 29: Corresponding line sections of the phase images presented in Figure 28

Figure 30 presents the analyzed line sections from the 2D-FFTs from the phase image of Figure 29. To analyze this line sections quantitavely, a Gaussian Fit was used and is represented by the red line in the individual diagrams. The analysis for the air dried fiber in the reciprocal 2D-FFT space revealed a value of 1.22 μm^{-1} for the full line and 34.88 μm^{-1} for the dashed line. The values in real space are 29 nm for the dashed line, which corresponds to the width of the individual microfibrils, and 0.8 µm for the full line, which corresponds to the width of the wrinkles. The analysis for the flash dried fiber revealed 48 nm for the microfibril width and 0.94 µm for the typical width of the observed wrinkles. These values from the 2D-FFT are in good agreement with the values found from the manual analysis of Figure 29.

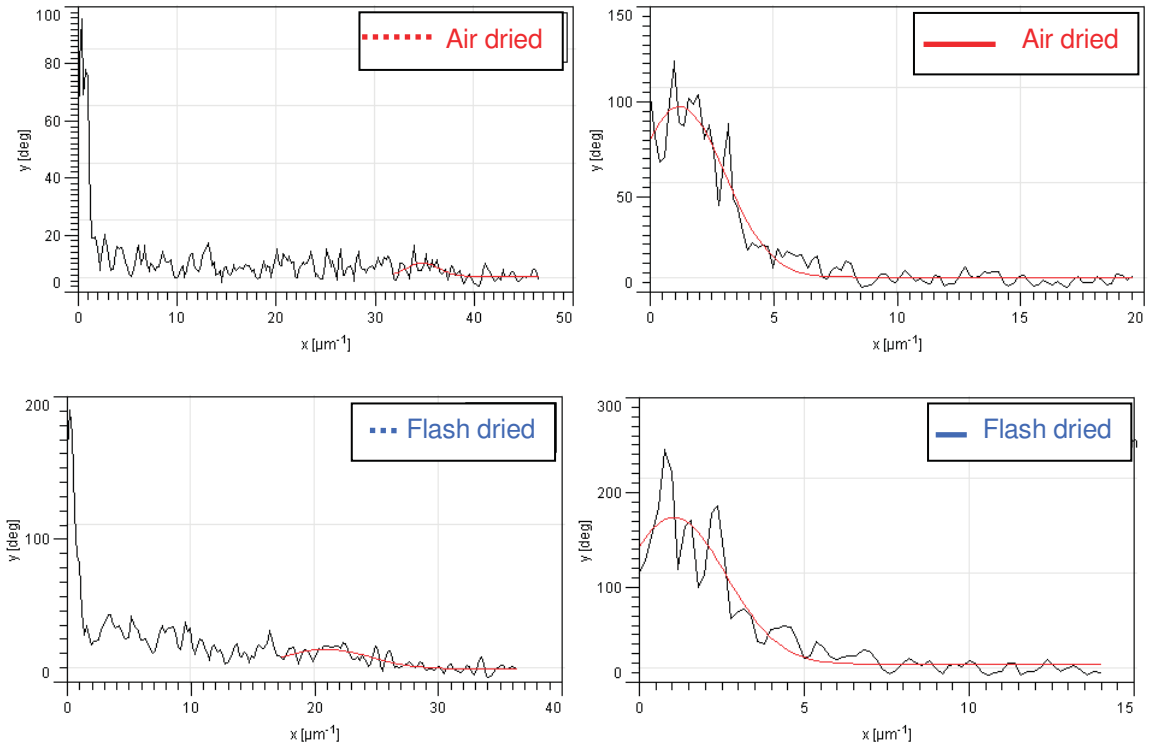

Figure 30: Analysis of the 2D-FFTs from the Insets of Figure 29
Left: Analysis in fiber direction
Right: Analysis perpendicular to the fiber direction)

Figure 31 shows the corresponding phase distribution histograms of Figure 28. The histograms offer two separated clear peaks. The left one of the peaks corresponds to the dark features and the right one to the bright cellulose fibrils. The investigation of the phase distribution images suggested that the surface material is identical because the phase shift between the two peaks is comparable. The difference of the mean peak positions is 51° for the air dried fiber and 79° for the flash dried fiber. The difference in these values is suggested to be due to different humidity during the measurements. The air dried fiber was measured at 30% humidity. The flash dried fiber instead at 67% humidity. The spike in the histogram of the air dried fiber corresponds to an imaging artifact.

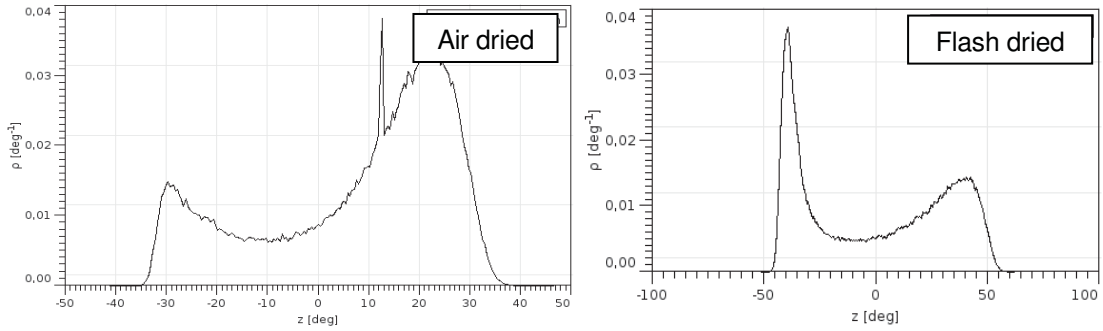

Figure 31: Phase distribution histograms from Figure 28
Left: Air dried fiber
Right: Flash dried fiber

5.1.2 Ozone treatment

It is known that ozone reacts mainly with lignin and removes it from the surface. The ozone is breaking unsaturated bonds thereby increasing the hydrophilicity of the fibers [27]. Thus, ozone treatment of the fiber could have an effect on the fiber surface.

Figure 32 shows a topographic and a phase image of the trace signal of an ozone treated fiber. The rms-roughness of the ozone treated fiber is 140 nm in the 5µm x 5µm image. This roughness is higher than for the untreated fibers. The cellulose fibril content has been determined to 58 ± 2%. This value is comparable to the flash dried fiber. The cellulose fibrils run again perpendicular to the main axis of the fibril bundles.

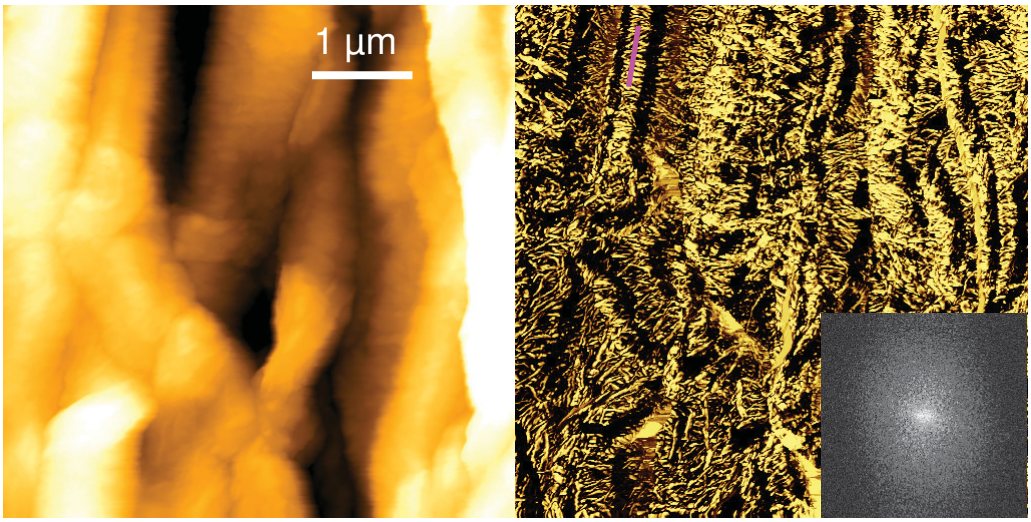

Figure 32: Height and phase image of an ozone treated fiber
Left: Height image (z-scale: 500 nm)
Right: Corresponding phase image (φ-scale 90 °)
Inset: Corresponding 2D-FFT from the phase image

Manual analyses of the line scans across the fibrils yield a fibrillar width of 41 ± 12 nm (see Figure 33). The surface structure looks very similar to the untreated fibers, especially to the flash dried fibers.

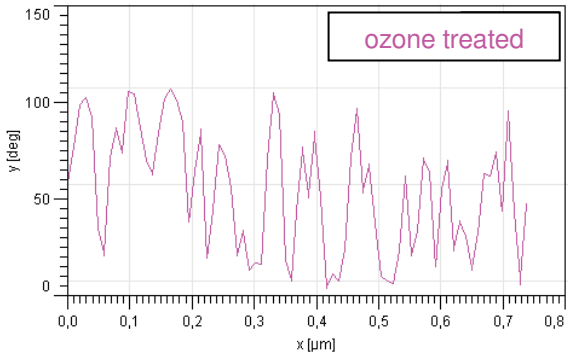

Figure 33: Corresponding line section from Figure 32

Figure 34 shows the phase distribution histogram of the bleached fiber. Again two clear separated peaks can be seen. The peak on the left side corresponds to the surrounding matrix. The right one indicates the bright fibrils. The fiber was measured at a humidity value of 25%. In comparison to the untreated fiber the distance between the main peak positions is higher (about 95 degrees). This could be explained with the increasing hydrophilicitiy of fibers as it is described by Koljonen et al. [27].

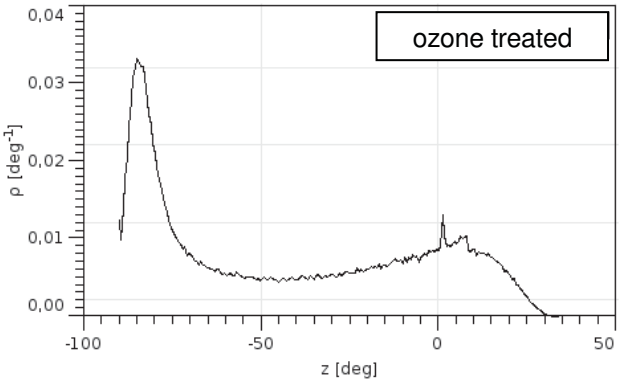

Figure 34: Phase distribution histogram of Figure 32

The AFM-phase imaging demonstrated that it is possible to visualize the individual cellulose fibrils and their arrangement on the fiber surface. The alignment of the microfibrils is perpendicular to the wrinkles. Simple fiber drying methods had no strong influence on the morphology of the fiber surface. Ozone treatment leaded to an increasing hydrophilicity of the fiber surface.

5.2 Investigation of cross-sections of man-made textile fibers

5.2.1 Viscose

Figure 35 and Figure 36 show TEM and AFM images of a Viscose fiber with the typical cross-sectional shape having the distinctive recess. The TEM and the AFM images are in good agreement. The pore structure is visible in TEM and AFM. It is possible to distinguish between a core and a shell area. The pores are mainly concentrated in the core area. The shell area of 1-2 µm thickness is more or less pore free. The analysis of Figure 36 offers the sight of two typical pore types. On the one hand, there are few huge pores with typical dimensions of 85 ± 17 nm for the minimum bounding size and 190 ± 100 nm for the maximum bounding size (marked with red circles in the height image of Figure 36). On the other hand, there are lots of tiny pores, which are smaller then 60 nm in diameter. The typical dimensions of these pores determined from the phase image of Figure 36 are 26 ± 10 nm for the minimum bounding size and 50 ± 20 nm for the maximum bounding size. Their aspect ratio is 1.9 ± 0.5.

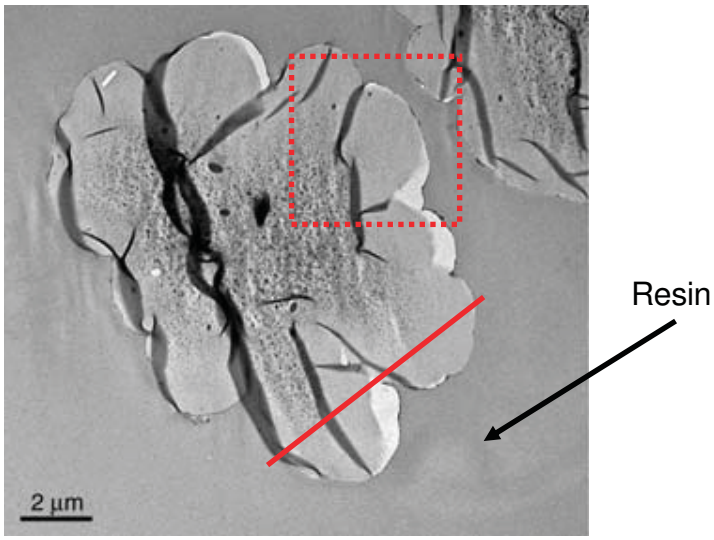

Figure 35: TEM image of a Viscose cross-sectional sample (from [20])

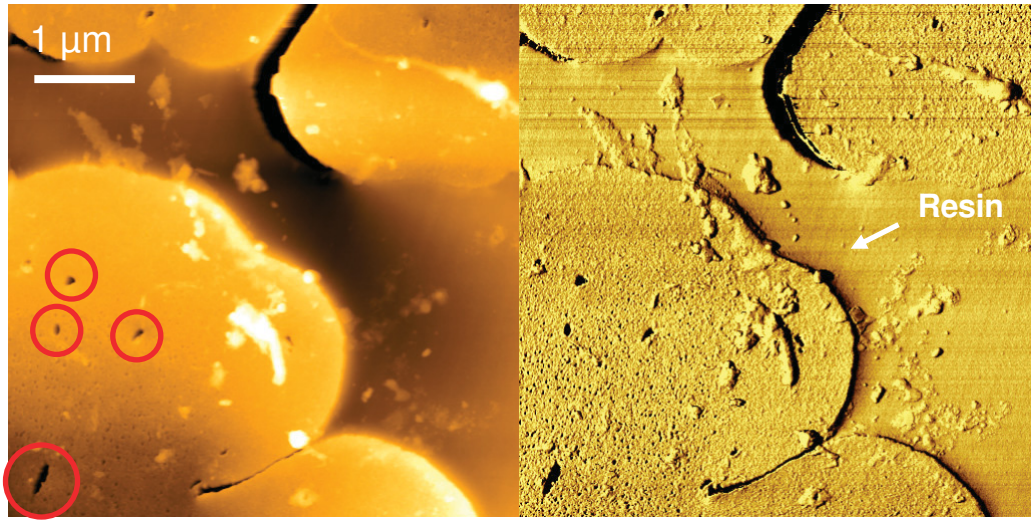

Figure 36: Large scale image of a Viscose fiber cross-sectional sample
Left: Height image (z-scale: 150nm)
Right: Corresponding phase image (φ-scale: 20 °)

Figure 37 shows a closer view of the core area which visualizes the tiny pores. The rms-roughness of the 1µm x 1µm height image is 8.3 nm. The visible bright features in the height image are isoprene or dirt. They are excluded from further consideration. An analysis of the pore fraction reveals that 11.1% of the image are pores (dark in the phase image). The typical dimensions are 15 ± 11 nm for the minimum bounding size and 28 ± 23 nm for the maximum bounding size. The aspect ratio is 2.0 ± 0.6. Figure 38 shows the corresponding diagram of bounding size analysis. The abscissa of the diagram corresponds to the maximum bounding size. The ordinate corresponds to the minimum bounding size. The linear fit represents the aspect ratio of the pores. The steeper the slope of the fit is the higher is the aspect ratio, which belongs to more elongated pores.

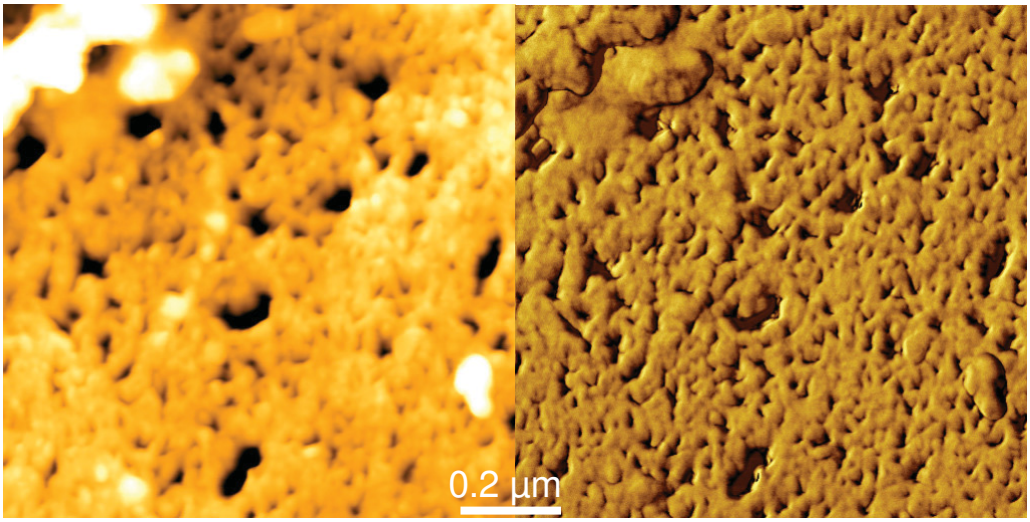

Figure 37: 1µm x 1µm AFM images of a Viscose cross-sectional scan
Left: Height image (z-scale: 50nm)
Right: Corresponding phase image (φ-scale: 30 °)

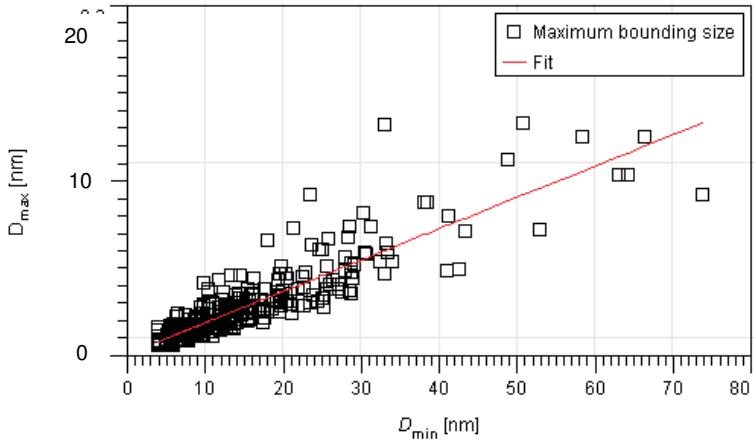

Figure 38: Diagram of D_{max} over D_{min} determined from Figure 37.

Figure 39 shows a longitudinal cross-section of a Viscose fiber. The recess of the typical Viscose cross-sectional shape is shown. The red line in Figure 35 gives an idea of the possible fiber cutting direction. The phase image shows an identical contrast in all three sections, indicating that the structure in all three sections is the same. Section I seems to contain some tiny pores in the lower left part of the image. In that case it would be possible to distinguish between the core and the shell area, but this is not as easy as in the cross-sectional scans because it is unknown at which position the fiber is exactly cut. It is assumed that the AFM image is located in an area as it is marked in Figure 35. Thus, there should be only a few huge pores and some tiny pores.

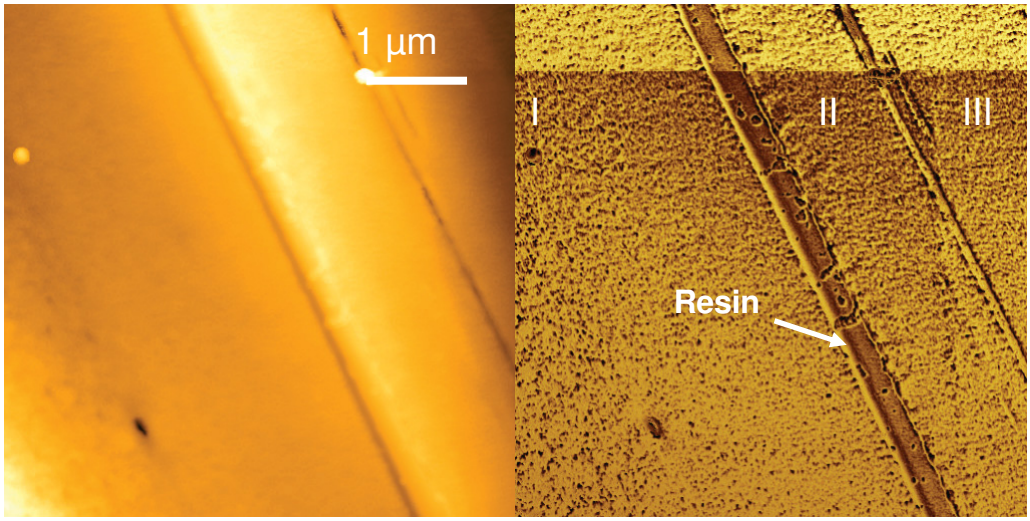

Figure 39: Viscose longitudinal section
Left: Height image (z-scale: 250 nm)
Right: Corresponding phase image (φ-scale: 20°)

Figure 40 presents a closer look at a Viscose longitudinal section. No huge pores are visible in this image. The phase image offers some tiny dark pores. The area fraction of the pores is about 4.7%. The typical dimensions are 23 ± 11 nm for the minimum bounding size and 36 ± 16 nm for the maximum bounding size. The aspect ratio is 1.7 ± 0.5. Figure 41 shows the corresponding diagram from the bounding size of the phase image. The diagram is similar to Figure 38, except that the bounding size is a little higher.

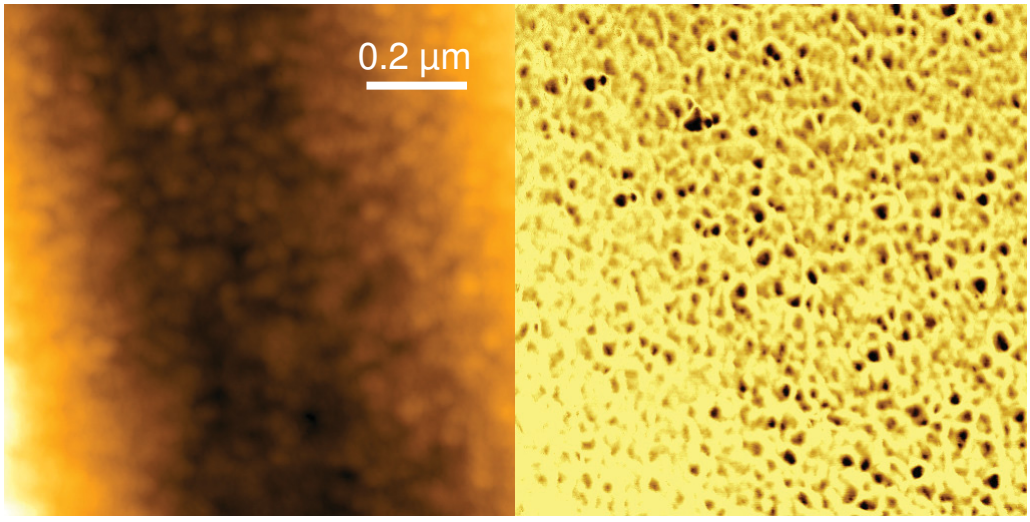

Figure 40: 1µm x 1µm AFM image of a Viscose longitudinal section
Left: Height image (z-scale: 50 nm)
Right: Corresponding phase image (φ-scale: 5°)

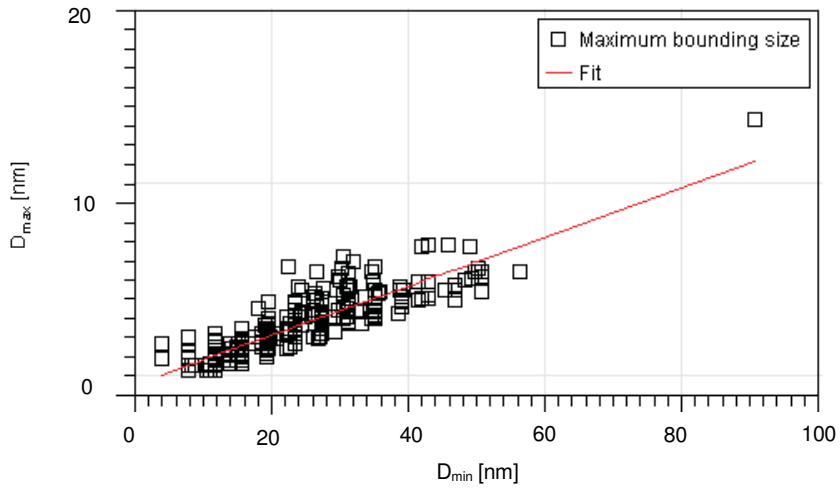

Figure 41: Diagram of D_{max} over D_{min} determined from Figure 40

The analysis of the Viscose fiber revealed that there is a difference between the core and the shell region. The shell area is free of detectable pores. The pores in the core are classified. There are few huge pores with an aspect ratio of about 2 and lots of tiny pores with nearly the same aspect ratio. The huge pores have typical diameters which are larger than 80 nm.

5.2.2 Modal

Figure 42 shows a comparison of some cross-sectional TEM and AFM scans of Modal fibers. Again there is a good agreement between the AFM and the TEM images. The pore structure is clearly visible by both techniques. There is also a difference between the core and the shell of the fiber. The analysis of the huge pores reveals 74 ± 40 nm for the minimum bounding size and 169 ± 98 nm for the maximum bounding size. The corresponding aspect ratio is 2.3 with a standard deviation of 0.8. The aspect ratio is larger than the one calculated from the Viscose fibers. Also, the scattering of data is larger, although there have been more pores used for the statistical calculation.

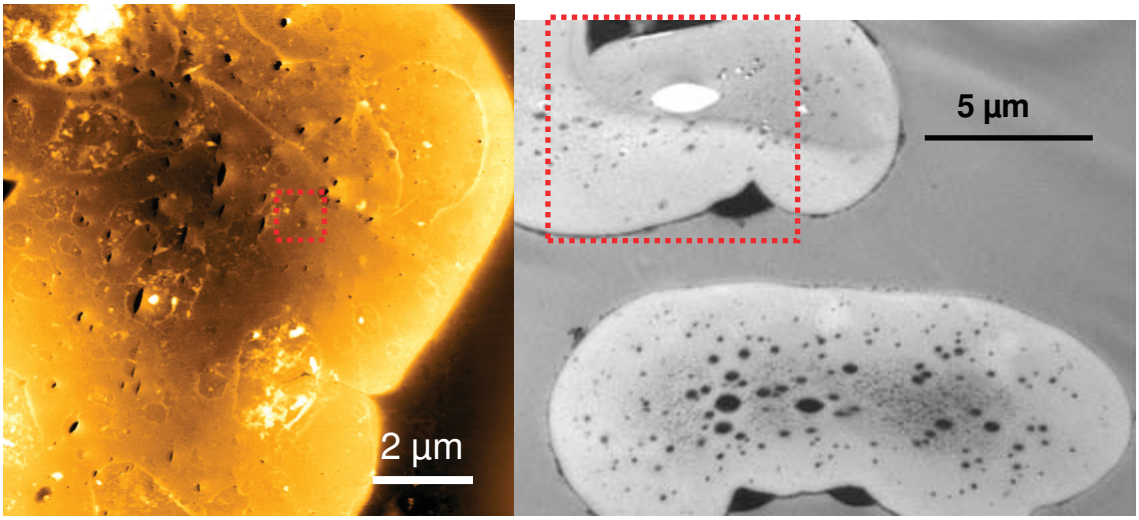

Figure 42: Cross-sectional scans of a Modal fiber
Left: AFM height image (z-scale: 100 nm)
Right: TEM image (from [20])

Figure 43 presents a zoom into the area marked in the AFM image of Figure 42. The typical dimensions of the tiny pores in the marked area in the phase image of Figure 43 are 9 ± 4 nm for the minimum bounding size and 16 ± 9 nm for the maximum bounding size. The dimensions of the tiny pores are a little bit smaller than the one calculated from the Viscose fiber. The aspect ratio is 1.8 ± 0.5 which is similar to the data from the Viscose fiber. Figure 44 shows the corresponding diagram of the individual pores from the box marked in the phase image of Figure 43.

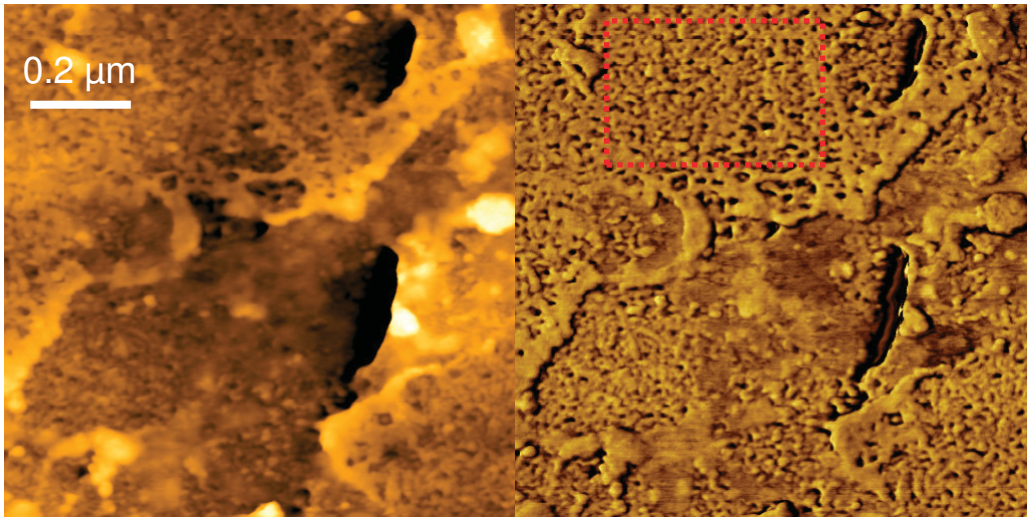

Figure 43: Zoom into the area marked in Figure 42
Left: Height image (z-scale: 40 nm)
Right: Corresponding phase image (φ-scale: 20 °)

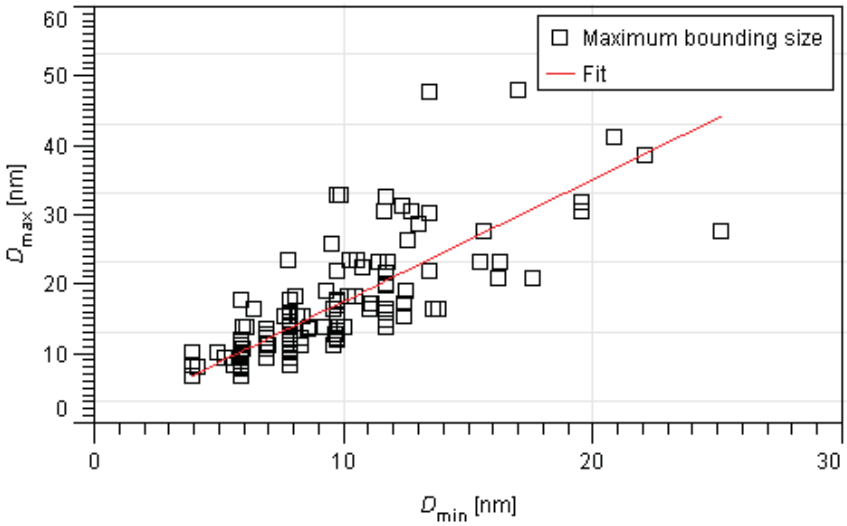

Figure 44: Diagram of D_{max} over D_{min} determined from the box masked in the phase image of Figure 43.

Figure 45 shows height images from large scale longitudinal cross-sections of Modal fibers. The images show several elongated pores that are completely filled with isoprene and some isoprene even expanded above the surface of the cut. Manual analysis of these pores leads to typical dimensions of 1.15 ± 0.4 µm for the maximum bounding size and 0.3 ± 0.1 for the minimum bounding size. The aspect ratio is 3.9 ± 0.7.

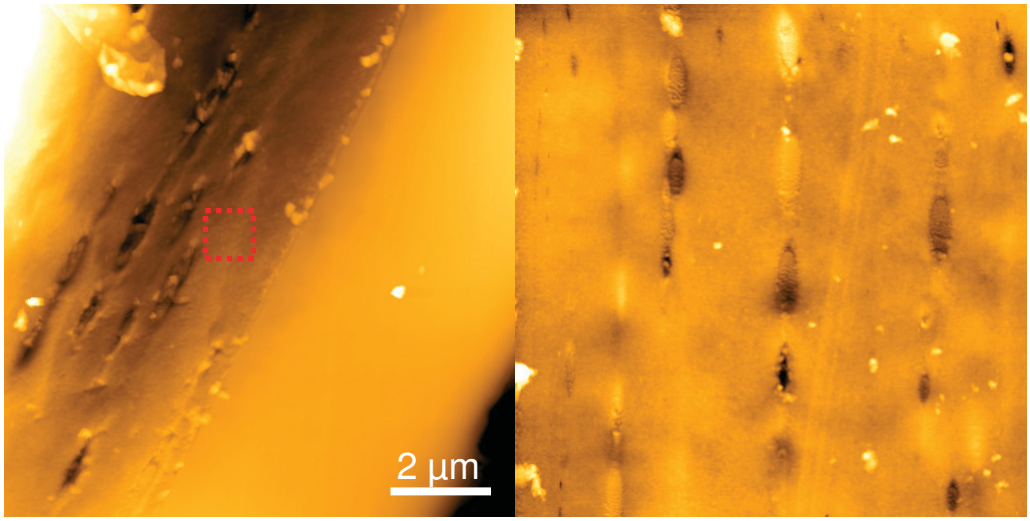

Figure 45: 10µm x 10µm topography images of longitudinal cross-sections of Modal fibers
Left: Height image (z-scale: 200 nm)
Right: Height image (z-scale: 100 nm)

Figure 46 shows a zoom into the marked area in Figure 45. Due to the small phase contrast it was not possible to determine the pore size and shapes automatically from the complete image. Manual analysis yields 26 ± 8 nm for the minimum bounding size and 36 ± 11 for the maximum bounding size. The aspect ratio is 1.4 ± 0.2. A semi-automatic calculation was also done with reducing the pore size to one pixel from the edge to separate the individual pores. The resulting diagram is represented in Figure 47.

The semi-automatic analysis of the phase image presented in Figure 46 yields 17 ± 8 nm for the minimum bounding size and 28 ± 13 nm for the maximum bounding size. The aspect ratio is 1.7 ± 0.4. The semi-automatically revealed values for the pores are smaller, because small grains were neglected by full manually analysis and the pores were manually reduced a little bit to separate the individual pores. One pixel corresponds to 2 nm. Therefore the minimum bounding size is recalculated to 21 ± 8 nm and the maximum bounding size is 32 ± 13 nm. The aspect ratio decreases to 1.5 ± 0.3.

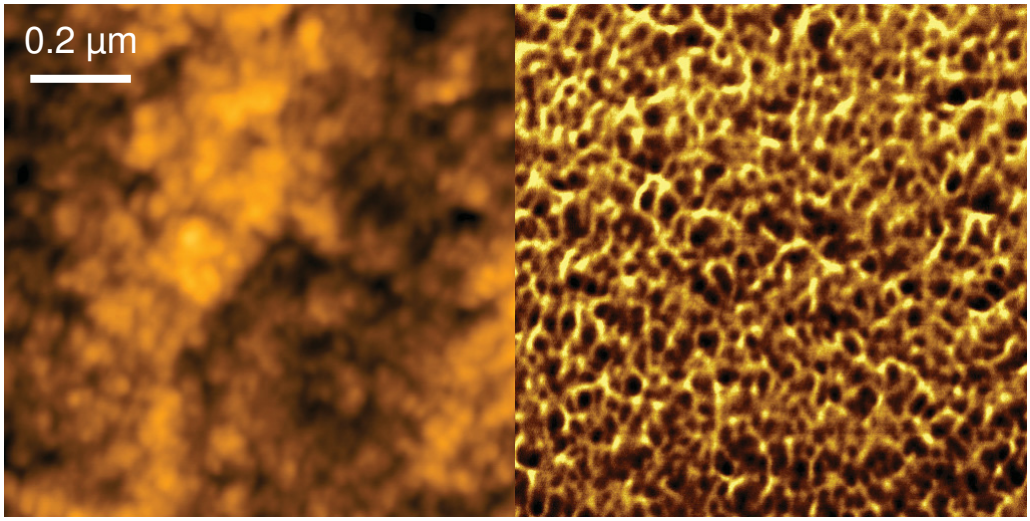

Figure 46: 1µmx1µm AFM image of the area marked in Figure 45
Left: Height image (z-scale: 20 nm)
Right: Corresponding phase image (φ-scale: 5°)

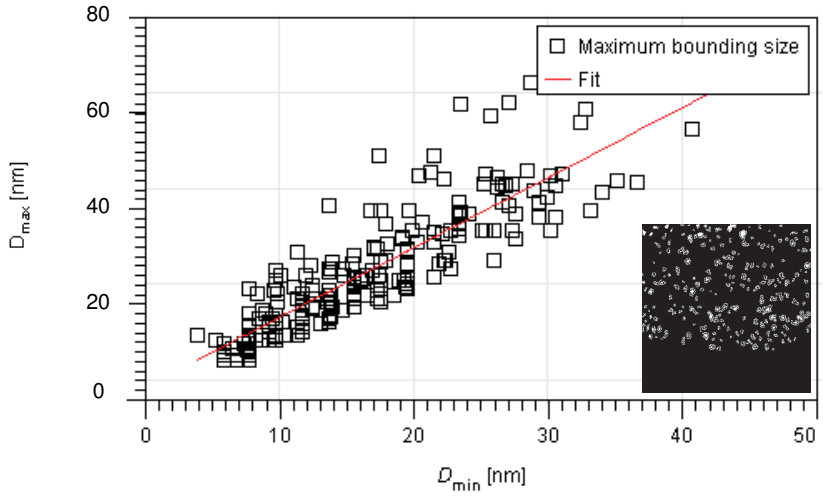

Figure 47: Diagram of D_{max} over D_{min} determined from Figure 46
Inset: Used mask for calculation

The analysis of the Modal fiber revealed that there is a difference between the core and the shell, but not as clear as it was observed in the Viscose fiber. The core area reveals most of the huge pores. The shell area reveals also some huge pores, but they are smaller in size and in number. The huge pores reveal an aspect ratio of about 2 for the cross-sections and an aspect ratio of about 4 for the longitudinal cross-sections. The analysis of the tiny pores yields a value slightly below 2, for both, cross-sections and longitudinal cross-sections. This analysis clearly reveals that the huge pores are strained in fiber direction. This was not observable for the tiny pores.

5.2.3 TENCEL®

Figure 48 presents large scale AFM and TEM images of a cross-sectional sample of a TENCEL® fiber. Both images show no pores. That means that there are no huge pores existing since they would be visible in the height image at this scale. The morphological structure observable in the large scale height image looks homogenous. The TEM and the AFM image fit perfectly. The diameter of the fiber seen in Figure 48 is up to 15 µm. Also the skin area is visible.

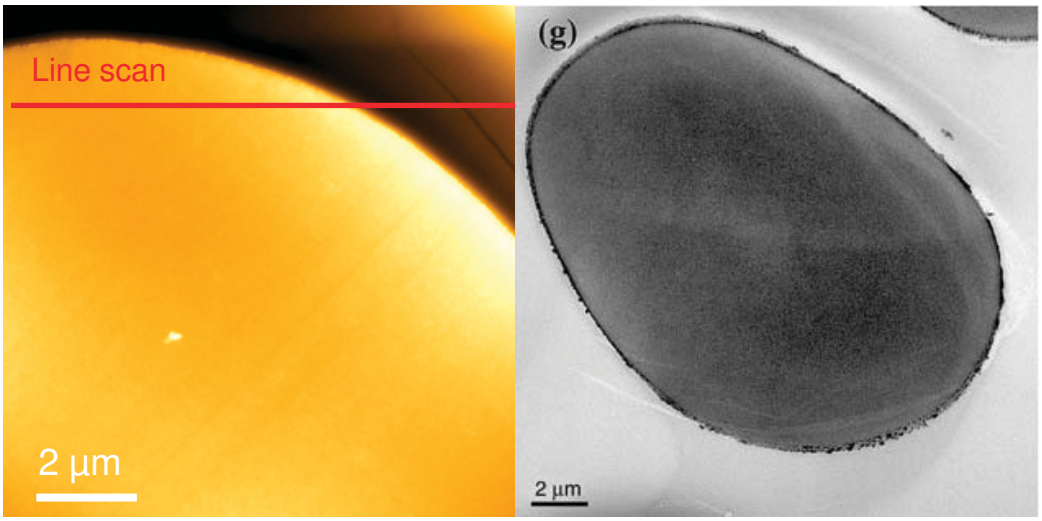

Figure 48: Large scale images of TENCEL® cross-sections.
Left: AFM height image (z-scale: 100 nm)
Right: TEM image(from [20])

Figure 49 shows a line scan from the AFM height image of Figure 48. It is clearly visible that the fiber protrudes from the resin. This was also observed for all the other fibers and helps with the location of the fiber on the sample surface. The reason may be humidity in the laboratory, due to which fibers are swollen.

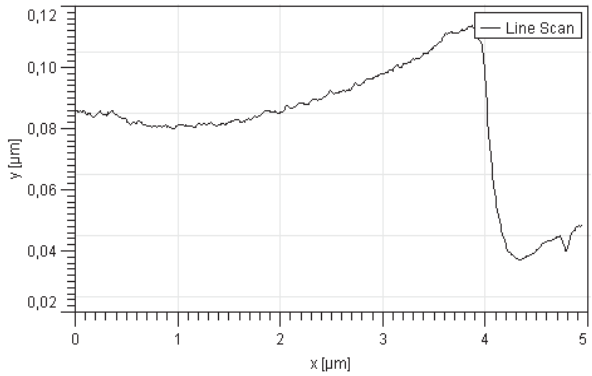

Figure 49: Corresponding line scan of Figure 48

Figure 50 represents a zoom into the cross-section of a TENCEL® fiber on the nanometer scale. It reveals a homogenous spongy structure. The rms-roughness of the height image is 0.8 nm. The analysis of the 2D-FFT of the phase image (see Figure 51) reveals preferential feature distances from 45 nm to 68 nm depending, on the direction. The difference in the directions of Figure 51 is may be due to inhomogeneous distribution of the pores inside the fiber.

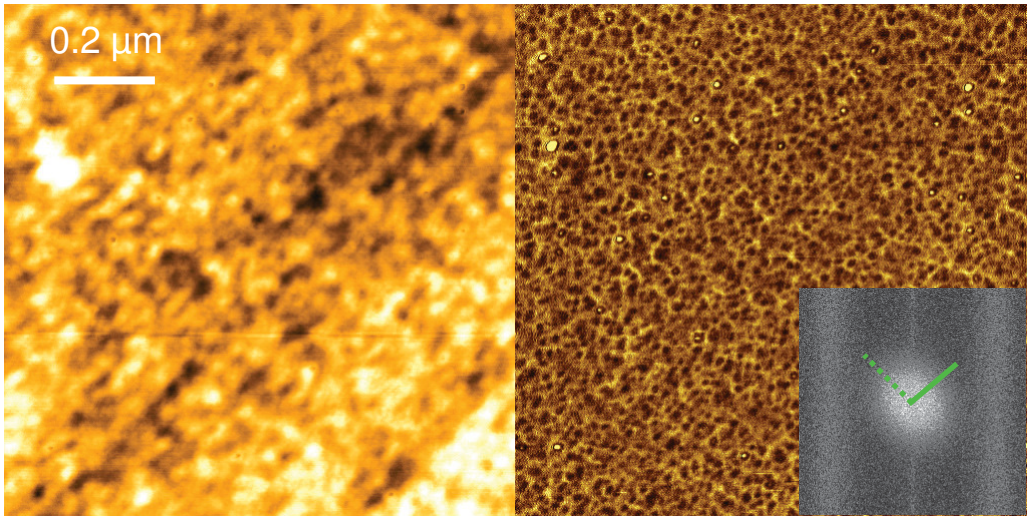

Figure 50: Small scale images of a TENCEL® cross-section
Left: Height image (z-scale: 5 nm)
Right: Corresponding phase image (φ-scale: 5 °)
Insert: Corresponding 2D-FFT from the phase image

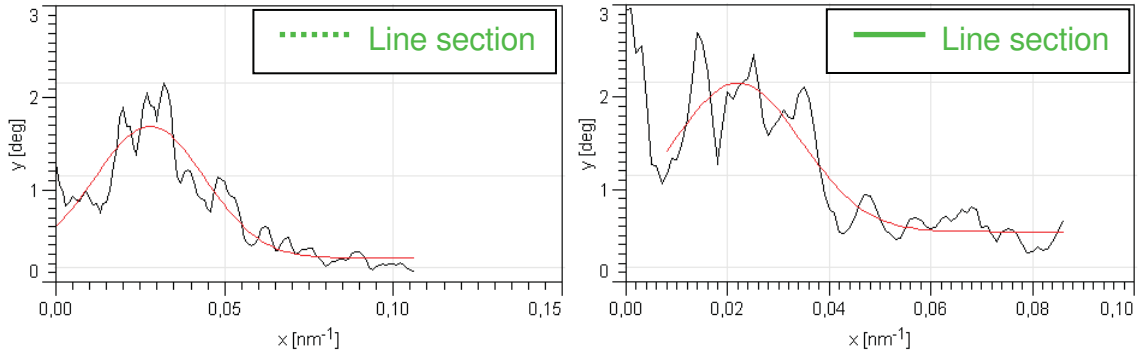

Figure 51: 2D-FFT analysis in different directions determined from the Insert in Figure 50

Figure 52 shows longitudinal sections of the TENCEL® fiber. The fiber reveals several elongated protrusions running parallel to the fiber axis. The typical dimensions of the protrusions are about 1800 nm by 200 nm. The large scale image offers no difference between the core and the skin area of the fiber. These protrusions are not typical for these fibers. The reason could be a preparation artifact due to the microtome cutting process.

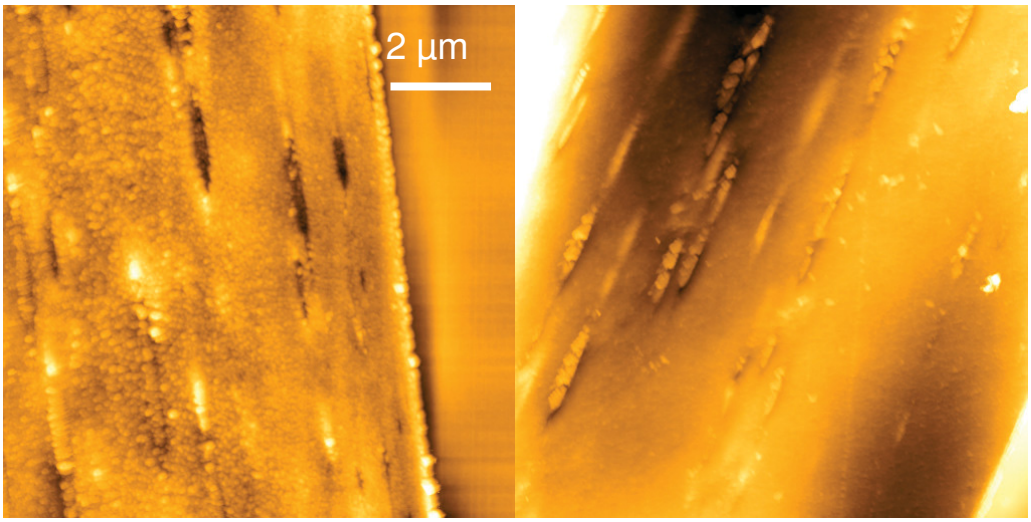

Figure 52: Large scale images of TENCEL® longitudinal cross-section
Left: Height image (z-scale: 50 nm)
Right: Height image (z-scale: 200 nm)

Figure 53 is a small scale image of the longitudinal cross-section of the TENCEL® fiber. The phase image reveals the same spongy structure seen in the cross-sectional samples. This structure was visible in the trace and the retrace signal of the phase image. The average aspect ratio of the dark features is about 1.7 with a standard deviation of 0.5. The typical dimensions of these features are 45 ± 25 nm for D_{max} and 27 ± 15 nm for D_{min}. The area fraction of the dark features - suggested to be pores - is about 16%.

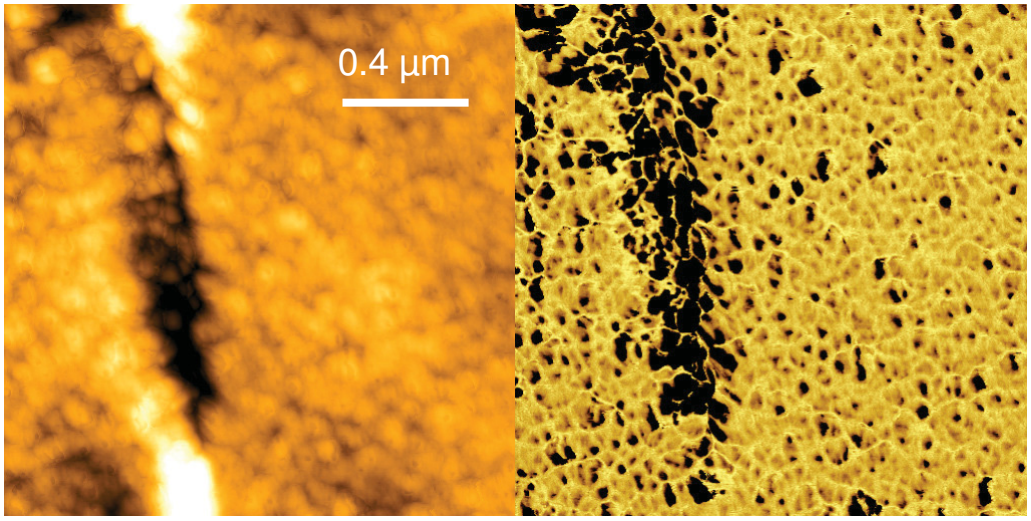

Figure 53: Small scale image of a TENCEL® fiber
Left: Height image (z-scale: 20 nm)
Right: Corresponding phase image (φ-scale: 10 °)

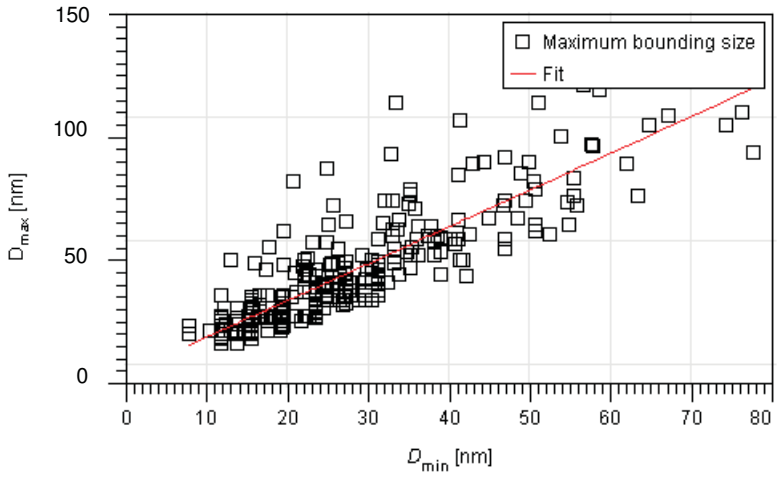

Figure 54: Diagram of D_{max} over D_{min} determined from Figure 53

The analysis of the pores in the TENCEL® fiber reveals that there are no pores larger than 60 nm diameter. A higher magnification reveals that there is a well defined structure on the nanometer scale. This defined structure looks like a sponge, which contains lots of tiny pores.

The textile fiber investigations presented in this part of the thesis are only representing the latest data. Actually the measurements of the last two years were focusing on analyzing TENCEL® cross-sections. Previous measurements investigated the fine pore system of the TENCEL® fibers to realize the water retention of the fiber. Therefore, measurements were performed to find out a difference between the core and the shell as it is reported in [20]. The AFM measurements yielded high resolution images of the TENCEL® fibers. Especially the sample preparation for AFM needed to be optimized to reveal the desired resolution without imaging artifacts, like isoprene that is oozed out or influences from the microtome cutting process. In addition to the work on the fiber surface (presented in [4]) measurements were extended to longitudinal cross-sections.

6. Summary and outlook

This study presents results of Atomic Force Microscopy (AFM) measurements of native and regenerated cellulose. By means of AFM topography and phase imaging it was possible to investigate the surface structure of single paper fibers and cross-sectional samples of various textile fibers.

The clear resolution difference between the height and the phase mode measurements was demonstrated at single paper fibers. Main bundles of microfibrils and individual microfibrils itself were observed. It was possible to visualize the microfibrils and the surrounding linkage. The results are supported by Scanning Electron Microscopy (SEM) measurements done at the FELMI in Graz. The phase image reveals the distribution of the microfibrils. A mean microfibril diameter ranges from 27 to 44 nm. The diameter of the main bundles of microfibrils is about 300 nm. This was also found in previous studies [9]. The alignment of the microfibrils is more or less perpendicular to the main bundles.

A second investigation was aimed at the consequences of different treatments on fiber morphology. Different drying methods were tested to determine which method has the potential to be a standard for transporting the samples between the laboratories. It was shown that there is no strong influence of the drying method on the morphology of the fiber surface. First measurements on ozone treated fibers revealed that the morphology of the fiber is similar to one of non-treated fibers. However, a change in the hydrophilicity of the treated fiber surface was determined by means of phase imaging. This is in a good agreement with the literature [27].

This preliminary study will be expanded in the future including more samples with different surface treatments. It is also planned to carry out the measurements under controlled environmental conditions.

Ongoing measurements will be continued especially on prepared cross-sectional samples studying fiber-fiber bonds. These measurements combine the overview information of the ultra microtome technique and the high resolution of the AFM technique. This combination is perhaps able to reveal the underlying mechanism for the fiber-fiber bond.

Future measurements will be done with tips covered by different metal coatings or tips functionalized with certain molecules [28]. This will allow determining the forces between AFM tip and fiber surface revealing a material's contrast. These measurements should reveal how much strength is possible to achieve in a paper sheet. Maybe it will also be possible to clearly distinguish between hemicellulose and

lignin on the fiber surface with choosing the right molecules for functionalizing the tip. This technique is expected to reveal new insights into the surface structure and chemistry of paper fibers depending on the fabrication conditions and post fabrication treatment.

The investigations of the textile fibers demonstrated that it is possible to visualize the inner structure of the different man-made cellulose fibers. This was possible by filling the pores with isoprene instead of water. The isoprene leads to a material contrast that allows distinguishing the pores. The studies revealed that it was possible to observe the difference of the inner structure of the Viscose, Modal and TENCEL® fibers. The measurements perfectly fit the revealed TEM data found in the literature [20].

Analyzing the Viscose fiber revealed that the inner structure of the fiber has a difference between the core and the shell area. The core area is porous, wheras the shell area is more or less free of detectable pores. This was also found in the literature [20]. With AFM it was possible to analyze both the huge pores which were seen in the TEM images, and the tiny pores, which were only seen superficially in the TEM images.

The Modal fiber showed again huge and small pores. It was possible to analyze both pores. Also a difference between the core and the shell was observable. The core area contains most of the pores. In the shell area, there are only a few smaller pores present. This is also comparable to data found in the literature [20]. The pore diameters widely ranged from a few nanometers to a few hundred nanometers.

Measurements at the TENCEL® fiber showed a very homogenous pattern. No huge pores were found. Therefore, the measurements focused on observing the nanostructure of the fiber. It was possible to reveal a spongy structure on the nanometer scale. This was seen in cross-sections as well as in longitudinal cross-sections.

Longitudinal cross-sections are shown in this study. The idea of the longitudinal cross-sections was to visualize the geometry of the pore shape along the fiber axis. The aim was to find a certain asymmetry of the pores in the individual fibers. Analysis yielded that the huge pores from the Modal are not as round as the pores from the Viscose fiber. The previous work revealed that it is difficult to produce a good image, because it is almost unknown where the fiber is exactly cut. An enhancement would be a quick analysis of the AFM samples with SEM for marking interesting fibers.

Ongoing measurements of longitudinal cross-sections are aimed to study the influence of the microtome cutting on the sample and to analyze the nanostructure of the

TENCEL® fiber. Also measurements on samples with an OsO_4 treatment will be analyzed to find out what happens to the fiber, because this treatment increases the material's contrast in TEM images. It is known that the OsO_4 leads to a hardening of the surface. Therefore, it is even harder to achieve a good phase contrast in AFM-TM measurements. Nanoindentation could be applied as a complementary technique to study material's contrast and the influence of the OsO_4 treatment [29].

7. References

[1] Voith paper, http://www.voithpaper.com/vp_d_faser_verppapiere_sackpapier.htm, February 2008.

[2] Mondi, http://www.mondigroup.com/desktopdefault.aspx/tabid-164, February 2008.

[3] Tianello, http://www.tianello.com/mm5/merchant.mvc?Screen=CTGY&Store_Code=T&Category_Code=SH, February 2008.

[4] P. Hosemann, "Characterization of cellulose fibers using Atomic Force Microscopy", Diploma Thesis, Leoben, 2004.

[5] History of Lyocell, http://everything2.com/index.pl?node_id=1489629, February 2008.

[6] Lenzing, http://www.lenzing.com/fasern/de/textil/4180.jsp, February 2008.

[7] Wikipedia, "Cellulose", http://en.wikipedia.org/wiki/Cellulose, February 2008.

[8] J. H. Bos, et al. (editors), "Das Papierbuch, Handbuch der Papierherstellung", 1. Auflage 1999, EPN Verlag, ISBN 90 11 060385, Seite 29 f.

[9] J. Simola, P. Malkavaara, R. Alén, J. Peltonen, "Scanning probe microscopy of pine and birch kraft pulp fibres", Polymer **41** (2000) 2121-2126.

[10] Universität Uitrecht, Biomolecular Research http://www.nmr.chem.uu.nl/bijvoet_brochure/brochure.html.

[11] Cellulose, http://www.lsbu.ac.uk/water/hycel.html.

[12] Physikalisch-Chemisches Praktikum I, http://chemie-graz.at/PC-1_Adsorption.pdf.

[13] Textillexikon, http://www.kimmich-modeversand.de/textillexikon.html#a330.

[14] R. J. Colten, et al. (editors), "Procedures in Scanning Probe Microscopy", John Wiley and Sons, 1998.

[15] Schematic principle of AFM http://www.farmfak.uu.se/farm/farmfyskem-web/instrumentation/images/afm.gif, February 2008.

[16] Tapping mode, http://www.nature.com/nmat/journal/v6/n6/images/nmat1925-f1.jpg, February 2008.

[17] Gwyddion homepage, http://www.gwyddion.net.

[18] Gwyddion user guide, http://gwyddion.net/documentation/user-guide/ Februar 2008.

[19] FFTW library, http://www.fftw.org/, February 2008.

[20] M. Abu Rous, E. Ingolic, K. C. Schuster, “Visualisation of the fibrillar and pore morphology of cellulosic fibres apllying TEM”, Cellulose 13 (2006) 411-419.

[21] L.Reimer, G. Pfefferkorn, “Rasterelektronenmikroskopie“, 2. Auflage (Springer Berlin 1977).

[22] Schematic principle of SEM, http://www.purdue.edu/REM/rs/graphics/sem2.gif.

[23] Wikipedia TEM, http://de.wikipedia.org/wiki/Transmissionselektronenmikroskop.

[24] Nanosensors, http://www.nanosensors.com/products_overview.html#ATEC.

[25] J. Gustafsson, L. Ciovica, J. Peltonen, “The ultrastructure of spruce kraft pulps studied by AFM and XPS”, Polymer 44 (2003) 661-667.

[26] V. J. Morris, A. R. Kirby, A. P. Gunning, “Atomic Force Microscopy for Biologists”, Institute of Food Research, Norwich, UK 1999.

[27] K. Koljonen, M. Österberg, L. S. Johansson, P. Stenius, “Surface chemistry and morphology of different mechanical pulps determined by ESCA and AFM”, Colloids and Surfaces A 228 (2003) 143-158.

[28] J. C. Bastidas, R. Venditti, J. Pawlak, R. Gilbert, S. Zauscher, J. F. Kadla, “Chemical force microscopy of cellulosic fibers”, Carbohydrate Polymers 62 (2005) 369-378.

[29] W. Gindl, J. Konnerth, T. Schöberl, “Nanoindentation of regenerated cellulose fibres“, Cellulose 13 (2006) 1-7.

8. Acknowledgements

My special thanks go to

Ao. Univ. Prof. Dipl. Phys. Dr.rer.nat. Christian Teichert for his patient expert guidance, for the trust to my person and the correction of this work.

Dipl. Ing. Dr. techn. Kurt Christian Schuster, **Lenzing AG** for his intense cooperation and his helpful discussions.

Ao. Univ. Prof. Dr. Robert Schennach for his intense cooperation.

Dipl. Ing. Lisbeth Kappl for preparing the paper samples and her helpful discussions.

Dipl. Ing. Dr.techn. Ulrich Hirn for his helpful discussions.

Dr. phil. Elisabeth Ingolic, Research Institute for Electron Microscopy and Fine Structure Research (FELMI) the Graz University of Technology for preparing the microtome cuts.

Dr. mont. Dipl. Ing. Gregor Hlawacek and **Dr. mont Dipl. Ing. Christian Hofer** for their helpful discussions and support with the AFM measurements.

Dipl. Ing. Peter Hosemann for introducing me into the world of fibers.

Ing. Heinz Pirker and **Peter Moharitsch** for the technical support.

Heide Kirchberger and **Magdalena Ottrin** for the administrative support.

Christian Stecher, **Nurdogan Gürkan** and **Thomas Klünsner** for the good working atmosphere.

DDr. Isabella Pali for the correction of this work.

My colleagues

My family

Furthermore, my special thanks go to everyone who helped me in the course of my diploma thesis and who I did not mention explicitly.

9. Abbreviations

AFM	Atomic Force Microscopy
SEM	Scanning Electron Microscopy
TEM	Transmission Electron Microscopy
OM	Optical Microscopy
FFT	Fast Fourier Transformation
ATR-FTIR	Attenuated Total Reflection Fourier Transformation Infra Red Spectroscopy
TM	Tapping Mode